ACS OMEGA

Open Access

http://pubs.acs.org/journal/acsodf

Article

Loading of STING Agonist into Lipid Nanoparticles Boosts Dendritic Cell Activation

Ana RS Ribeiro,[‡] Ander Eguskiza,[‡] Hieu-Hoa Dang, Theresa Neuper, Michael Stefan Unger, Laura Rodriguez Comas, Markus Steiner, Helene Sieberer, Nadja Zaborsky, Richard Greil, Mireia Vilar I Hernandez, Pascal Jonkheijm,* Roberto Fiammengo,* and Jutta Horejs-Hoeck*

Cite This: *ACS Omega* 2025, 10, 58465−58479

Read Online

ACCESS | Metrics & More | Article Recommendations | Supporting Information

ABSTRACT: Activation of the STING pathway is crucial for antitumor immunity, but targeting the STING receptor therapeutically remains a challenge due to inefficient intracellular delivery of its agonists. Here, we explore the potential of FDA-approved lipid nanoparticles (LNPs), used in Spikevax COVID-19 vaccine, to increase the uptake of a cGAMP analog (cG^sA^sMP) to dendritic cells (DCs) and induce cell activation. These LNPs are highly reproducible, effectively encapsulate cG^sA^sMP, and are easily scalable. We show that cG^sA^sMP LNPs are efficiently internalized by DCs *in vitro*, and the cargo is released into the cytoplasm, which strongly enhances STING activation and DC maturation. Furthermore, we introduce an *in vitro* model of tumor-associated human DCs that mimics the DC phenotype observed in cancer patients. When applied to this model, cG^sA^sMP LNPs successfully reprogram tumor-associated DCs toward an active state, thus emphasizing their potential for cancer immunotherapy. Overall, this work presents a novel and scalable approach utilizing LNPs to deliver cyclic dinucleotide-based STING agonists to counteract immune suppression in cancer.

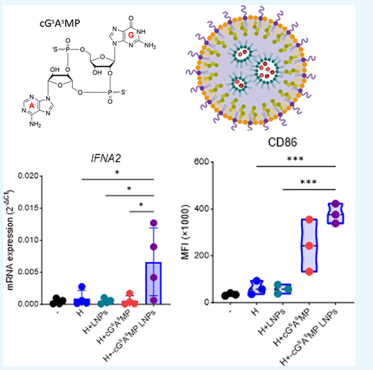

1. INTRODUCTION

Current immunotherapy strategies concentrate on harnessing the host immune system to destroy tumor cells through robust adaptive antitumor responses, with notable success in the treatment of both solid and hematological malignancies tied to the deployment of immune checkpoint blockade and chimeric antigen receptor T cells (CAR-T), respectively.[1,2] Nonetheless, the progress in activating tumor-specific T-cell responses alone has been slow because that activity depends on each patient's immune context and, in particular, on signals received from innate immune cells, such as dendritic cells (DCs).[3−5] DCs are specialized antigen-presenting cells (APCs) that, by surveilling and sampling all tissues, can recognize molecular patterns associated with pathogens (PAMPs) or cellular damage (DAMPs), thus prompting appropriate immune responses and playing a key role in fighting diseases such as cancer.[6] In the tumor context, DCs can sustain specific antitumor immune responses by activating cytotoxic $CD8^+$ T cells and by priming $CD4^+$ T cells.[4,5,7] However, in the case of solid tumors, an immunosuppressive tumor microenvironment (TME) often develops, which contributes to immune evasion by severely compromising the functions of various immune cells, including DCs.[8,9] Specifically at the DC level, there is evidence that the TME promotes the upregulation of immune checkpoint molecules, coinhibitory markers and immunosuppressive factors in cancer patients, resulting in regulatory T-cell polarization that prevents potent antitumor immunity.[8,10]

In human blood, two major subsets of conventional dendritic cells (cDCs) are recognized: $CD141^+$ cDC1 and $CD1c^+$ cDC2.[11] While cDC 1s are established as key mediators of antitumor immunity through efficient cross-priming of $CD8^+$ T cells,[12] recent evidence highlights an equally important role for cDC 2s. Beyond presenting antigens to both $CD4^+$ and $CD8^+$ T cells,[13] cDC 2s can transfer tumor-derived antigens to resident DCs in lymphoid tissues, thereby amplifying antitumor T cell responses.[14]

A critical signaling pathway in antitumor immunity involves the activation of the STimulator of InterferoN Genes (STING) receptor. Upon binding to viral or free cellular DNA, cyclic guanosine monophosphate-adenosine monophosphate synthase (cGAS) catalyzes the synthesis of cyclic guanosine monophosphate-adenosine monophosphate cGAMP or GMP-AMP, which is the natural ligand for STING receptor in mammals.[15] Upon cGAMP binding, STING is activated and mediates subsequent signaling through phosphorylation of tank-binding kinase 1 (TBK1) and interferon (IFN)-regulatory factors,which prompts a type I IFN-dependent inflammatory response.[16−18] Type I IFN

Received: June 27, 2025
Revised: October 1, 2025
Accepted: November 17, 2025
Published: November 21, 2025

production by DCs through STING activation has been shown to support effective cross-priming of $CD8^+$ T cells toward antitumor-specific immunogenicity in several *in vivo* tumor models.[19,20] Furthermore, preclinical studies have shown that activation of this pathway through endogenous or exogenous agonists is an essential trigger of antitumor immunity.[16,21]

However, targeting STING by endogenous delivery of cGAMP or other natural cyclic dinucleotides (CDNs) remains problematic. cGAMP is unable to passively diffuse through the plasma membrane due to its negative charge and highly hydrophilic nature. Moreover, although the organic anionic transporter SLC19A1 was recently identified as the first cGAMP transporter, this protein is not known to be part of the dominant cGAMP import mechanism for any primary cell type.[18,22,23] In addition, cGAMP is highly susceptibile to rapid hydrolysis by enzymes that are prevalent in plasma.[22−24] In consideration of the aforementioned factors, the natural ligand of STING, cGAMP, is not an appropriate choice for therapeutic purposes when used in its free state. Yet, intratumoral administration of the free form of a synthetic nonhydrolyzable analog of cGAMP, ADU-S100, also did not yield satisfactory clinical results. Thus, exploration of novel drug delivery platforms enhancing therapeutic efficacy and overcome pharmacological barriers is urgently needed.[25]

Nanoparticle delivery platforms hold significant promise in enhancing the effectiveness of loaded antigens and adjuvants by adjusting the pharmacokinetic and distribution profiles while improving cargo delivery to site of action.[26,27] Because appropriate uptake of STING ligands is of critical importance for enhancing effective vaccine responses, in recent years, several efforts to improve cGAMP delivery have focused on different nanoparticle-based systems.[28,29] Often these approaches have yielded promising results *in vitro* and *in vivo* but stymied by nonreproducible synthesis or limited clinical translational potential of the delivery system, for example in the case of using permanently cationic lipids for encapsulation of cargo.[30−35] Ionizable lipid nanoparticles (LNPs) are the most clinically advanced nonviral platform for delivery of nucleic acids such as siRNA or mRNA and have been successfully employed as a vaccine against COVID-19.[36,37] However, their ability to deliver CDNs, such as the STING ligand, to immune cells has not been reported. In fact, formulation of CDNs in LNPs poses additional challenges compared to nucleic acids because CDNs are much smaller molecules than the mRNA used in Spikevax vaccines and have only two negative charges, potentially resulting in weaker interactions of the CDNs with the ionizable lipids of LNPs.[38] A recent study on LNPs containing adamantyl-based ionizable lipidoids revealed minimal encapsulation of CDNs and yet showed potent activation of immortalized STING reporter cells,[39] suggesting LNPs may be used to formulate CDNs.[40]

In this study, we demonstrate the capability of the LNP formulation employed in the Spikevax vaccine as a carrier for cyclic dinucleotides. We successfully encapsulate and deliver the cGAMP analog 2′3′-cGAM(PS)2 (Rp/Sp) (cG^sA^sMP) to dendritic cells, which induces a STING-dependent adjuvant function. Furthermore, since tumor-infiltrated DCs exhibit an phenotype altered by the immunosuppressive tumor microenvironment (TME), we introduce a novel *in vitro* platform of tumor-associated human DCs to validate the adjuvant potential of the encapsulated STING agonist. We demonstrate that the phenotype displayed by in vitro-conditioned DCs closely mirrors that of DCs found in lung cancer tumors, emphasizing the physiological relevance of this model for the screening of therapeutic agents.[41] Unlike murine models, which often fail to fully replicate human immune responses due to interspecies differences, the use of primary human dendritic cells (DCs) and *in vitro*-conditioned DCs offers a complementary, but clinically relevant model system that directly reflects human biology. This is particularly critical in evaluating the therapeutic potential of STING agonists, that displays different polymorphisms among species, limiting the translation potential of murine studies to human applications.

2. EXPERIMENTAL SECTION

2.1. Synthesis and Characterization of LNPs. Lipid nanoparticles were formulated as previously described with minor variations as follows.[42] Briefly, the aqueous solution containing 1 mg/mL cG^sA^sMP (Invivogen) was prepared in 10 mM citrate buffer, pH 4, and the organic solution containing a total lipid concentration of 15.5 mg/mL corresponding to SM-102 (TargetMol Chemicals Inc.), DSPC (Echelon Biosciences), cholesterol (TargetMol Chemicals Inc.) and DMG-PEG (Echelon Biosciences); molar distribution 50:10:38.5:1.5 was prepared in absolute ethanol. Subsequently, 56 μL of the aqueous solution was rapidly mixed into 18.6 μL of the organic solution by manual pipetting for 30 s, resulting in a final aqueous to organic ratio of 3:1. For the synthesis of the empty LNPs, 10 mM citrate buffer pH = 4 was used as an aqueous solution. The ratio of cG^sA^sMP to lipid was 1:6 (w/w). LNPs were then transferred to a 4 mL 50 kDa Amicon ultrafiltration device (Sigma-Aldrich) and washed twice with 0.22 μm filtered Phosphate Buffered Saline (PBS) for (10 min, 2700×*g*, 4 °C). LNPs were resuspended in PBS and were ready for use. Fluo-cGAMP LNPs were prepared by the same strategy using cyclic (adenosine monophosphate-8-(2-[fluoresceinyl]-aminoethylthio)guanosine monophosphate) (c-(Ap-8-Fluo-AET-Gp), BIOLOG Life Science Institute). LNP size distribution was measured at 25 °C by dynamic light scattering (DLS) using a Litesizer 500 instrument (Anton Paar) in PBS at a final lipid concentration of 4 μg/mL using the backscatter measurement angle (173°), 5 repeated measurements. Zeta potential was measured in 0.1× PBS using the same dilution as for the size measurement. For stability studies in biological media, LNPs were dispersed in RPMI 1640 or RPMI 1640 supplemented with 10% fetal bovine serum (FBS) at a final lipid concentration of 20 μg/mL and the solutions were stored at room temperature (RT) until measurement. Nanoparticle tracking analysis (NTA) was performed using a NanoSight NS300 (Malvern Panalytical Ltd.) at a final lipid concentration of 40 μg/mL in PBS, RPMI 1640, and RPMI 1640 supplemented with 10% FBS.

The loading efficiency of cG^sA^sMP LNPs was determined by measuring the absorbance of cG^sA^sMP at λ=254 nm after disruption of LNPs in 75% isopropanol and comparing to a calibration curve at various cG^sA^sMP concentrations in a matched matrix containing a fixed amount of LNPs to remove the contribution of the lipid mixture. The percentage loading efficiency was calculated as the ratio between the amount of cG^sA^sMP in the LNPs and the total amount of cG^sA^sMP in the LNP formulation. Loading efficiency of Fluo-cGAMP LNPs was determined by measuring the fluorescence intensity at 490/530 nm and comparing to a calibration curve at various Fluo-cGAMP concentrations using a microplate reader (Tecan Infinite 200).

https://doi.org/10.1021/acsomega.5c06105
ACS Omega 2025, 10, 58465−58479

2.2. NfκB-luc TLR4 Reporter Gene Assay. Potential endotoxin contamination in cG^SA^SMP-loaded LNPs and respective controls was assessed through an NF-κB-luc TLR4 reporter gene assay, as described by Schwarz et al.[43] Briefly, after seeding HEK293 cells (mycoplasma negative, culture passage 5−15) at a density of 1.5×10^5 in 500 μL per well in DMEM medium (SigmaAldrich, Austria) supplemented with 10% fetal calf serum (FCS), 1% L-glutamine and 1% MEM nonessential amino acids, 100 U/mL penicillin and 100 mg/mL streptomycin, cells were allowed to rest overnight at 37 °C. Cells were then transfected using Lipofectamine 2000 reagent (Fisher Scientific, Germany) as per the manufacturer's instructions. 500 ng of DNA and 1.5 μL of Lipofectamine 2000 reagent were diluted in 25 μL of Opti-MEM (Gibco, Germany) and pooled with a suspension of Opti-MEM containing the plasmids of interest: NFkB luciferase reporter (kindly provided by Min Li-Weber and cloned into pGL3Neo) and a TLR4 receptor mix in a 4:1 ratio. The TLR4 receptor mix contains the expression plasmids for TLR4 (in pCDNA3), CD14 (in pCDNA3) and MD2 (in pEFBOS) (kindly provided by Medvedev and Douglas Golenbock) in a ratio of 3:1:1. After pooling the solutions, the tube was incubated at RT for 10 min before the transfection mix was added dropwise to the wells. After 24h, the cells were treated with defined concentrations of LPS or with 15 μg/mL of empty LNPs, cG^SA^SMP LNPs or respective free cG^SA^SMP content, and incubated overnight. After 22h of exposure to the formulations, supernatants were removed and cells were lysed in 100 μL of lysis buffer (100 mM potassium phosphate, 0.1% Triton X-100, 1 mM DTT). The lysates were then transferred in duplicates to white polystyrene flat-bottomed 96-well plates. Luciferase activity was measured in a Tecan Infinite 200 Pro microplate reader (Tecan, Austria), after injection of 50 μL of luciferase substrate by an automated dispenser.

2.3. Isolation of DCs. This study was conducted following the guidelines of the World Medical Association's Declaration of Helsinki. National regulations do not require informed consent in the case of anonymous blood cells that are discarded after plasmapheresis (buffy coats), thus no additional approval by the local ethics committee was required.

DCs were isolated from peripheral blood mononuclear cells (PBMCs) of buffy coats of healthy anonymous donors, provided by the Blood Bank Salzburg as reported previously.[44] PBMCs were obtained by gradient density separation with Histopaque-1077 (SigmaAldrich, Austria) and washed three times with PBS before proceeding to subset isolation by magnetic cell separation. Conventional type 2 DCs (cDC 2s) were isolated by applying negative selection followed by positive selection using a CD1c (BDCA-1)$^+$ DC isolation kit from Miltenyi Biotec, Germany. After isolation, cDC 2s which are hereafter referred to simply as dendritic cells (DCs) throughout the manuscript were cultured in RPMI-1640 medium (Sigma-Aldrich) supplemented with 10% heat-inactivated FCS; Biowest, France) and 1% L-glutamine (ThermoFisher Scientific, Germany).

2.4. Culture of Immune Cells and LNPs. After isolating DCs or PBMCs, cells were seeded at a density of 4×10^5/mL in 500 μL and rested for 1h at 37 °C. Subsequently, 500 μL of medium were added for uninduced controls or cells were treated with 500 μL of medium containing 30 μg/mL of empty LNPs, cG^SA^SMP LNPs, or the respective amounts of cG^SA^SMP to a final concentration of 15 μg/mL of LNPs, which is reported to be a well-tolerated dose by myeloid cells in vitro.[45] For a 15 μg/mL of LNPs, the cGAMP concentration is equal to 1.5 ± 0.30 μg/mL of cGAMP. After 22 h of stimulation, cells and supernatants were harvested for downstream phenotypical characterization.

2.5. Development of Tumor-Associated Regulatory DCs (mregDCs). H1437 cells were seeded in 24-well plates at an optimal cell density of 3×10^4 in RPMI medium supplemented with 10% heat-inactivated FCS and with 1% L-glutamine for 96 h. The supernatants were harvested and centrifuged for 10 min at 300×*g* before being added to freshly isolated cDC2 cultures. cDC 2s were seeded at 2×10^5 cells per well in 500 μL in 24 well plates and cDC 1s were seeded at 5×10^4 cells per well in 100 μL in 96 well V-bottom plates and then conditioned with cancer cell line supernatant at a 1:1 ratio to a final volume of 1 mL or 200 μL, respectively. After 24 h of incubation, cells and supernatants were collected for analysis of DC phenotypes.

2.6. Coculture Systems. To assess the impact of cG^SA^SMP LNP-loaded DCs on polarization of T cells cocultures of cDC 2s and CD4$^+$ T cells were established. Briefly, DCs were seeded at 1×10^5 cells per well in 250 μL in 48-well plates and incubated for 22h with cG^SA^SMP LNPs or respective controls in an equal volume, normalized to 15 μg/mL of LNPs. On the following day, CD4$^+$ T cells were isolated through negative selection using the Microbeads Cocktail II kit according to manufacturer's instructions (Miltenyi Biotech, Germany) and added in a ratio of 10:1 to unconditioned DCs or to mregDCs to a final volume of 1 mL. Cocultures were kept at 37 °C for 6 days before cells and supernatants were harvested to assess CD4$^+$T cell polarization via flow cytometry, and additional analysis of supernatants through multiplex-based detection of secreted soluble factors.

2.7. Immunophenotyping by Flow Cytometry. Analysis of differential expression of cell-surface markers was performed by flow cytometry and analysis of median fluorescence intensity (MFI) on a Cytoflex S (Beckman Coulter). Briefly, cells were washed in PBS before being stained in 30 μL of staining mix for 30 min in the dark at 4 °C to avoid photobleaching. After staining, the cells were washed and fixed with 4% paraformaldehyde (PFA) for 10 min at 4 °C, then washed once in PBS and resuspended in PBS + 2 mM EDTA for analysis. For characterization of T-cell polarization in the six-day coculture setting, samples were permeabilized when necessary, according to the manufacturer's instructions. Data analysis was performed using FlowJo 10.9 software and induction ratios (IR) were calculated for the mean of MFI between treated and the respective control group. The following antibody-fluorophore conjugates were used: CD86 AF488 (IT2.2, Cat#: 305414), ILT4 PE (42D1, Cat#: 338706), ILT3 PerCP-Cy5.5 (ZM4.1, Cat#: 333014), PD-L2 PE-Dazzle (24F.10C12, Cat#: 329617), CD40 AF700 (5C3, Cat#: 334327), CD1c BV421 (L161, Cat#: 331526), CD80 BV605 (2D10, Cat#: 305225) from Biolegend, ILT2 APC (HP-F1, Cat#: 17−5129 eBiosciences), HLA-DR BV510 (G46−6, Cat#: 563083) and PD-L1 PE-Cy7 (MIH1, Cat#: 558017) from BD-BioSciences and Fixable Viability Dye eFluor F780 (Cat#: 65−0865−18, ThermoFisher).

2.8. Cytometry by Time-of-Flight (CyTOF). In-depth characterization of exhaustion markers expression of the regulatory T-cell population was performed on three-day cocultures set up with 3×10^5 cDC 2s and 3×10^6 CD4$^+$ naïve T cells by single-cell mass cytometry). For each sample, 10 million cells were prepared following the manufacturer's

https://doi.org/10.1021/acsomega.5c06105
ACS Omega 2025, 10, 58465−58479

suggestions for the Maxpar Complete Human T Cell Immuno-oncology Panel Set (Standard BioTools, USA). For live/dead discrimination, cisplatin staining was performed using 500 μL of a 1:3000 diluted solution. Three million cisplatin-labeled cells were further processed and incubated with 34 antibodies from the T cell panel kit for 30 min at RT. After washing the cells, the samples were fixed using 1 mL of a 2% PFA solution (freshly diluted from 16% stock solution; Pierce, Thermo Fisher Scientific, USA) for 10 min at RT. All subsequent washing steps were performed with centrifugation at 800×*g*. For cell identification, the DNA intercalator iridium was used. The cells were incubated in a 1:4000 diluted iridium intercalator solution (Standard BioTools, USA) overnight at 4 °C. The samples were then resuspended in cell acquisition solution (CAS; Standard BioTools, USA) with spiked-in EQ beads (1/10 in CAS) to achieve a final cell concentration of 500 000 cells/mL. The suspension was filtered with a 30 μm cell strainer (Sysmex, Austria) and measured on a Helios mass cytometer (Standard BioTools, USA) equipped with a WB injector. Data analysis was performed using R. The mass cytometry data were cleaned up according to the cleanup strategy outlined in the technical note "Approach to Bivariate Analysis of Data Acquired Using the Maxpar Direct Immune Profiling Assay (Technical Note 400248 Rev 06, Standard BioTools) using R (Version 4.3.1), RStudio (2023.06.0 Build 421, Posit Software, PBC) and the R package "CytoExplor-eR".[46] All viable $CD3^+/CD4^+$ T cells were further analyzed using the R package Spectre.[47] Data were arcsin h transformed using a cofactor of 3. The data were clustered using the FlowSOM algorithm embedded in the Spectre package with metacluster size set to 6. For dimensionality reduction, the data were subsampled to 200,000 cells per sample and the t-SNE algorithm (included in the Spectre package) was used with perplexity set to 20 and theta set to 0.5. The following markers were used for clustering and dimensionality reduction: CD2, CD25, CD44, CD57, CD69, CD127, CD134, CD152, CD161, CD278, HLA-DR. The expression of exhaustion markers was normalized per cluster prevalence according to the following formula:

$$X\_norm = (1 - 0) \times (X - \min)/(\max - \min)$$

2.9. Immunofluorescence and Confocal Microscopy. For intracellular uptake analysis of cGAMP in human DCs, cells were seeded as described above (5×10^5 cells/mL per well) and stimulated with LNPs, free Fluo-cGAMP or the above formulated Fluo-cGAMP LNPs for the indicated times. Thereafter, half of the supernatant was discarded and the resuspended cells were directly spun onto objective slides at 600 rpm for 3 min using a Cytospin 4 centrifuge (Epredia, Dreieich, Germany). Sample regions were marked with a Hydrophobic Barrier Pap Pen (Thermo Fisher Scientific) after drying and the cells were immediately fixed with 4% PFA for 15 min at RT. Samples were then transferred to a wet staining chamber and washed three times with PBS. Cells were incubated for 15 min at RT in the dark with the fluorescence-labeled cell membrane dye WGA-CF640R (Wheat Germ Agglutinin, Biotium #29026). Afterward cells were washed with PBS and incubated for 1 h at RT in the dark with the nucleus counterstain 4′,6-diamidino-2-phenyl-indol-dihydro-chlorid (DAPI 1:2000, MBD0015, Sigma-Aldrich). Cells were subsequently washed 3 times with PBS and semidry mounted with glass coverslips in Pro-Long Gold Antifade Mountant (Invitrogen #P36934). For analysis of intracellular p-STING expression, cells were seeded (2.5×10^5 cells/mL per well) and stimulated with LNP particles, cG^sA^sMP LNPs (15 μg/mL of lipids) or free cG^sA^sMP, normalized to the respective batch encapsulation efficiency. After 18 h, most of the supernatant was carefully removed and cells were infused and fixed with PFA for 15 min at RT, using a final concentration of 3%. The fixed cells were harvested from the wells and centrifuged for 5 min at 2000 rpm. Supernatants were discarded and cell pellets were resuspended in PBS. Then, cells were spun onto object slides using the Cytospin centrifuge at 600 rpm for 5 min. After a short drying, sample regions were marked with a Hydrophobic Barrier Pap Pen, samples were transferred to a wet staining chamber and washed 2 times with PBS. Cells were permeabilized with 0.1% Triton X-100 (Sigma-Aldrich, #93443) for 10 min, followed by two washes with PBS. Unspecific binding sites were blocked with 2% bovine serum albumin (BSA) and 5% donkey serum (Sigma-Aldrich, #D9663) for 1 h at RT. Samples were incubated with primary rabbit antihuman p(Ser366)-STING (Cell Signaling Technology, #50907, 1:300) overnight at 4 °C. Thereafter, samples were washed extensively in PBS and incubated for 2 h at RT in the dark with secondary donkey antirabbit AF568 (Invitrogen, 1:1000) and nucleus counterstain DAPI (1:2000). Cells were subsequently washed 3 times with PBS and semidry mounted with glass coverslips in Pro-Long Gold Antifade Mountant. DCs were analyzed using a Zeiss Observer Z1 fluorescence microscope equipped with an Abberior Instruments STEDYCON unit for confocal and super-resolution STED microscopy. Representative confocal images were taken with a 100× oil objective (ROI: 50 × 50 μm or 30 × 30 μm) from single focal z-planes to visualize Fluorescein-labeled cGAMP signals and the intracellular expression of p-STING. All images were postprocessed with Fiji (ImageJ1.54f) and Microsoft PowerPoint.

2.10. ELISA. TNF-α, IL-10 and IL-6 ELISAs (Peprotech, United Kingdom) were performed on supernatants harvested from induced and uninduced DCs, according to the manufacturer's instructions.

2.11. Western Blot. Cells were lysed in 2x LaemmLi sample buffer (Bio-Rad, Vienna, Austria) supplemented with 5% beta-mercaptoethanol, and diluted 1:1 in 1× PBS. Samples were then submitted to size separation on a 4−12% NuPAGE Bis-Tris gel (Invitrogen, Vienna, Austria) and thereafter transferred onto a nitrocellulose membrane (0.45 μm). Following blocking of nonspecific binding sites with 5% skim milk for 1 h at RT under gentle agitation and washing, the membrane was incubated with the primary antibody, prepared in 5% BSA diluted in Tris-buffered saline containing 0.1% TWEEN20 (TBS-T) overnight at 4 °C under gentle agitation. After another round of washing, the membrane was further incubated with the appropriate secondary antibody conjugated with horseradish peroxidase (HRP) for 1 h at RT under gentle agitation. After washing, the membrane was incubated with West Pico PLUS chemiluminescent substrate (Thermo Fisher Scientific), and detection was performed with a ChemiDoc Imager (Bio-Rad). The following primary and secondary antibodies were used according to the manufacturer's instructions; p-STING (Cell Signaling, #19781, 1:1000) STING: 13647 (Cell Signaling, #13647 1:1000), B-actin: 4970 (Cell Signaling, #4970, 1:50 000) in BSA and secondary antibody anti rabbit (Cell Signaling, #7074, 1:2000) in milk.

2.12. mRNA Expression Analysis. TRI Reagent (SigmaAldrich, Austria) was used according to the manufacturer's

https://doi.org/10.1021/acsomega.5c06105
ACS Omega 2025, 10, 58465−58479

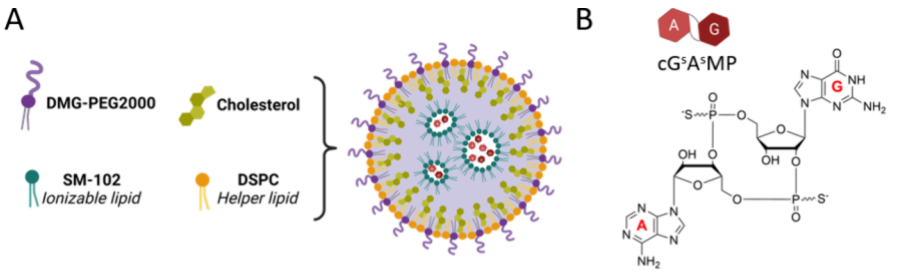

C

	Size (nm)	PdI	Zeta potential (mV)	Loading efficiency (μg cG^{S}A^{S}MP/mg lipid)
LNPs	150 ± 13	0.116 ± 0.017	-4 ± 4	-
cG^{S}A^{S}MP LNPs	137 ± 16	0.124 ± 0.018	0 ± 2	97.1 ± 20.1
Fluo-cGAMP LNPs	137 ± 12	0.112 ± 0.004	-24 ± 6	47.7 ± 21.1

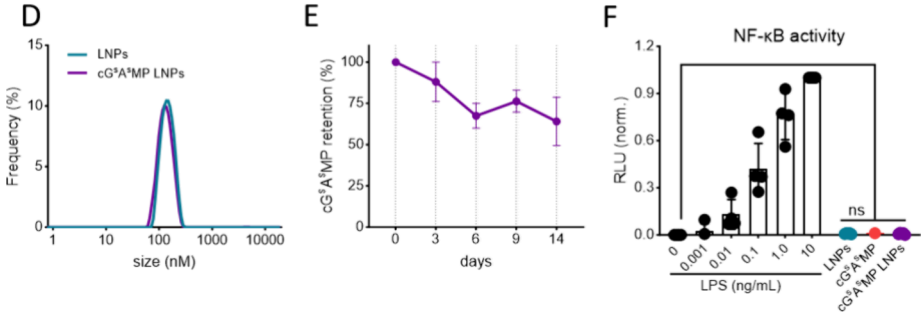

Figure 1. Synthesis and characterization of LNPs loaded with STING agonist cG^{S}A^{S}MP. (A) Schematic of the composition of cG^{S}A^{S}MP LNPs created with Biorender.com. (B) Chemical structure of the used cGAMP analog 2′3′-cGAM(PS)$_2$ (Rp/Sp) (cG^{S}A^{S}MP). (C) Physicochemical properties of LNP formulations from independent batches (empty LNPs n = 7 and cG^{S}A^{S}MP LNPs n = 8). Reported sizes are means ± s.d. from intensity distributions. Z-potential and loading efficiency values are means ± s.d. (D) Average size distribution based on dynamic light scattering of different batches of empty LNPs (n = 8) and cG^{S}A^{S}MP-loaded LNPs (n = 9). (E) Release studies of cG^{S}A^{S}MP from LNPs stored in PBS at 4 °C. Plotted values represent the average of 3 different batches, performed in 3 independent experiments. (F) Analysis of NF-κB activity using a luciferase-based assay in transfected HEK293 cells 24h after treatment with LPS, LNPs, or cG^{S}A^{S}MP LNPs, with the concentration normalized to 15 μg/mL of lipids and cG^{S}A^{S}MP normalized to respective batch loading efficiently (RLU = relative luminescence units). Plotted bars represent mean ± s.d. of four independent experiments (indicated by dots) containing two technical replicates each. For statistical analysis RM-ANOVA with a Tukey's post hoc test was performed.

instructions to extract total RNA content from cell pellets. mRNA was then reverse transcribed with RevertAid H Minus M-MuLV reverse transcriptase (ThermoFisher Scientific, Germany). Expression levels of genes of interest were determined by quantitative real-time PCR on a Rotor Gene 3000 instrument (Corbett Research, UK), using Luna Universal qPCR Master Mix (New England BioLabs, USA). mRNA expression was normalized to the expression of a housekeeping gene (RPLP0). Relative mRNA expression was calculated as $2^{-\Delta Ct}$, where the ΔCt value represents the difference between the threshold cycle (Ct) of the gene of interest minus the threshold cycle of the housekeeping gene. Specificity of primers was monitored via analysis of product melting curves. The following primer pairs were used: RPLP0 fwd 5′- GGC-ACC-ATT-GAA-ATC-CTG-AGT-GAT-GTG −3′, RPLP0 rev 5′- TTG-CGG-ACA-CCC-TCC-AGG-AAG-3′, IFNB fwd: 5′-CTG-CAA-CCT-TTC-GAA-GCC-TT-3′, rev: 5′-AAG-CCT-CCC-ATT-CAA-TTG-CC-3′, ISG15 fwd: 5′-CAT-CTT-TGC-CAG-TAC-AGG-AG-3′, rev: 5′-TGC-ATC-TGC-GCC-TTC-AGC-TCT-3′, CXCL10 fwd: 5′-GAA-TCC-AGA-ATC-GAA-GGC-CAT-CAA-GA-3′, rev: 5′-ATG-TAG-GGA-AGT-GAT-GGG-AGA-GGC-A3′, IFNA2 fwd: 5′-TCA-GCT-GCA-AGT-CAA-G-3′, rev: 5′-TCT-GCT-GGA-TCA-TCT-CAT-GG-3′

2.13. Endosomal Release through Metabolic Activity Assays. To investigate if endosomal escape was induced, freshly isolated DCs were seeded at a density of 1 × 10^5 cells per well in 250 μL in 48 well plates and coadministered with 15 μg/mL of LNPs and 1 μg/mL of gelonin (Enzo Life Sciences, Switzerland) for 22 h in a final volume of 500 μL. On the next day, cell pellets were transferred to 96-well V-bottom plates for metabolic activity assessment. Supernatants were discarded following 5 min of centrifugation at 300 g, the pellet was resuspended in 0.25 mg/mL of MTT working solution dissolved in serum-free medium before incubating the plate for 2 h at 37 °C. Thereafter, the plate was spun as described before and cells were resuspended in 8 mM ammonia in DMSO, after discarding the supernatants. After dissolution of MTT formazan crystals, the suspension was transferred to a transparent flat bottom plate and absorbance was measured at 570 and 650 nm using a Tecan Infinite 200 microplate reader.

https://doi.org/10.1021/acsomega.5c06105
ACS Omega 2025, 10, 58465−58479

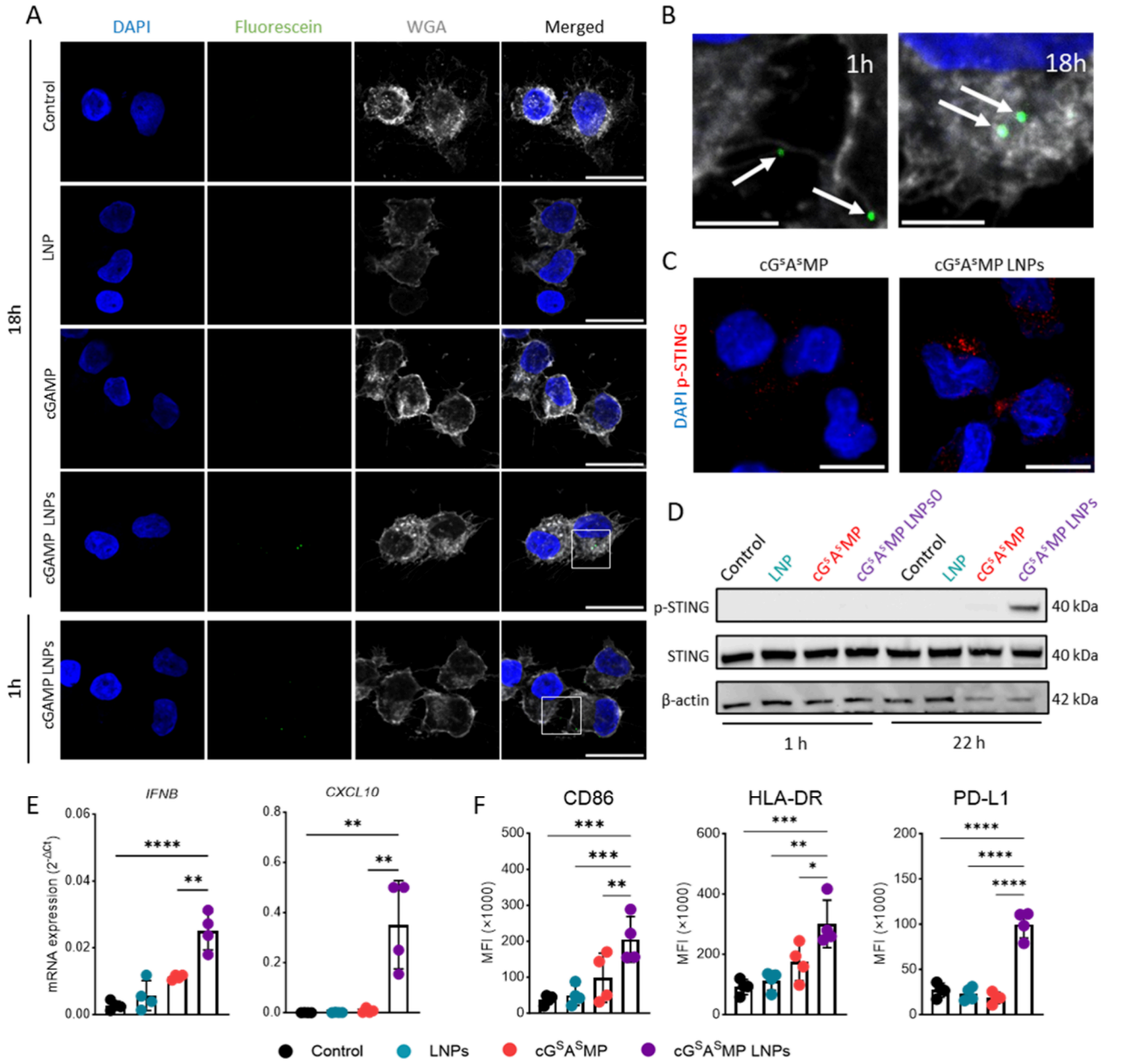

Figure 2. cG^{S}A^{S}MP-LNPs are efficiently taken up by human DCs and activate STING signaling following endosomal release. (A) Immunofluorescence staining of DCs stimulated with 15 μg/mL of empty LNPs and LNPs formulated with fluorescently labeled cGAMP (c-(Ap-8-Fluo-AET-Gp)) and corresponding dose of free fluo-cGAMP (1.04 μg/mL) after 1 and 18 h of incubation. Scale bar = 20 μm. (B) Zoomed-in images from panel A showing location of fluo-cGAMP LNPs in DCs after 1 and 18 h of incubation. DAPI was used to stain cell nuclei and WGA-CF640R to visualize cell membranes. Scale bar = 5 μm. (C) Immunofluorescence staining for phosphorylated STING (p-STING) in DCs treated with free cG^{S}A^{S}MP or cG^{S}A^{S}MP LNPs for 18 h. DAPI was used to stain cell nuclei. Scale bar = 5 μm. (D) Western blot analysis of STING phosphorylation and protein expression in DCs treated with 15 μg/mL of LNPs corresponding to 1.24 μg/mL of cG^{S}A^{S}MP for 1 and 22 h. (E) IFNB and CXCL10 mRNA expression in DCs incubated with cG^{S}A^{S}MP LNPs and respective controls after 22 h of incubation. (F) CD86, HLA-DR and PD-L1 expression, expressed as mean fluorescence intensity (MFI), in DCs incubated with cG^{S}A^{S}MP LNPs and respective controls after 22 h of incubation. Western blot and confocal images in panel A are representative of data obtained for two donors. Plotted values represent mean ± s.d. of two independent experiments using two different LNP batches for a total of 4 individual donors. Statistical analysis was performed using RM-ANOVA with Tukey's post hoc test. *$p \leq 0.05$, **$p \leq 0.01$, ****$p \leq 0.0001$).

3. RESULTS

3.1. Synthesis and Characterization of LNPs Loaded with STING Agonist cG^{S}A^{S}MP. We prepared LNPs loaded with cG^{S}A^{S}MP, a validated analog of mammalian cGAMP that is highly resistant to hydrolysis, by one-step nanoprecipitation (Figure 1**A and 1B**).[48] Similar to the production of mRNA-loaded LNPs, the LNPs were formulated in an acidic buffer to promote the formation of a complex between cationic ionizable lipid and cG^{S}A^{S}MP through ionic interactions.[36] Several batches were produced, and the average values of size, zeta potential, and loading efficiency for all formulations are shown in Figure 1C. Dynamic light scattering revealed a highly reproducible average hydrodynamic diameter of approximately 140 nm for cG^{S}A^{S}MP LNPs in phosphate-buffered saline (PBS), comparable to the size of unloaded LNPs (Figure 1**D**),

https://doi.org/10.1021/acsomega.5c06105
ACS Omega 2025, 10, 58465−58479

and visible in cryo-transmission electron microscopy (Supplementary Figure 1E). Zeta potential measurements indicate that the LNPs have a neutral charge at physiological pH, with no differences upon cG^{S}A^{S}MP loading. Moreover, LNPs successfully encapsulated the CDN analog while preserving the original nanoparticle composition of Spikevax vaccine. We obtained a loading of 97.1 ± 20.1 μg of cG^{S}A^{S}MP/mg lipid, corresponding to a loading efficiency of 56 ± 12%. This is a higher encapsulation efficiency than reported for comparable cationic liposome formulations.[39] Furthermore, the LNPs were stable upon storage (in PBS at 4 °C for 16 days) and showed no significant changes in nanoparticle size, with 64 ± 12% of the cG^{S}A^{S}MP still encapsulated after 2 weeks (Figure 1**E** **and**Supplementary Figure 1B). In addition, cG^{S}A^{S}MP LNPs were not significantly changing in size when incubating them for 22h in cell culture medium (Supplementary Figure 1C). Furthermore, when incubating cG^{S}A^{S}MP LNPs cell culture medium containing 10% FBS for up to 22h no significant increase in hydrodynamic diameter was observed indicating excellent resistance to protein adsorption (Supplementary Figure 1C and 1D). These physicochemical properties suggest that our LNPs may have limited clearance by phagocytic immune cells and could result in an increased half-life of the CDN cargo. Screening for lipopolysaccharide (LPS) content in novel formulations is particularly important when working with primary immune cells, such as the human blood-derived DCs we used in this study, because DCs can be activated by even a minute amount of endotoxin (e.g., LPS) contamination, often present in commercially available recombinant proteins.[49] To assess whether LNPs are contaminated with endotoxin, we transfected HEK293 cells with plasmids encoding the LPS receptor complex (TLR4, CD14 and MD2) and an Nf-κB-dependent luciferase reporter, and stimulated them with defined concentrations of LPS or with cG^{S}A^{S}MP LNPs or respective controls. Neither our formulated cG^{S}A^{S}MP LNPs nor empty LNPs or cG^{S}A^{S}MP alone induced Nf-κB activation, indicating that these constituents are not contaminated with LPS and therefore are well suited to evaluate STING-specific effects on primary human immune cells (Figure 1**F**).

3.2. Loading into LNPs Increases cG^{S}A^{S}MP Uptake and STING Activation. Since STING is an intracellular pattern recognition receptor (PRR), the efficiency of translocation of cGAMP or analog agonists from the endosome to the cytoplasm is highly relevant for the induction of subsequent immune signaling. Thus, to assess the immunogenic capacity of STING agonists, we examined LNP uptake, endosomal release and STING activation in human primary DCs, which are key players in the orchestration of potent adaptive immune responses. It is known that the cellular uptake of LNPs is essentially driven by the endocytic pathway, leading to accumulation of entrapped nanoparticles in early endosomes.[50] Consistent with this, we observed that stimulation of DCs with fluorescently labeled cGAMP (fluo-cGAMP) encapsulated in LNPs resulted in the accumulation of this adjuvant in the cells, while no signal was observed in cells incubated with free fluo-cGAMP (Figure 2**A**). Interestingly, after 1 h of incubation, the signal was mostly detected at the borders of the cell membrane or in the cellular dendrites, whereas at later time points the accumulation of fluo-cGAMP was clearly observed intracellularly (Figure 2**B**). Since the natural endocytic pathway leads to fusion of endosomes with acidic lysosomes, which contain several enzymes capable of disrupting the LNP structure and degrading the cargo, it is important that the majority of the functional molecules reach the cytosol before this degradation cascade is initiated.[51,52] We have therefore investigated wether the LNP formulation would improve translocation of the STING agonist to the cytosol by coadministering DCs with gelonin and the different LNP formulations or free cG^{S}A^{S}MP. In fact, gelonin is a highly potent polypeptide toxin that is taken up via the classical endocytic pathway and that is inert when trapped within endocytic vesicles, but toxic if released into the cytosol.[53] We observed that in the presence of gelonin, treatment of DCs with both LNPs and cG^{S}A^{S}MP LNPs led to impaired cellular metabolic activity, suggesting that LNPs promoted increased endosomal release of endosomal-entrapped gelonin (Figure 2**A**). Thus, LNPs are expected to promote cytosolic release of coformulated cG^{S}A^{S}MP as well.

Given that fluo-cGAMP LNPs are taken up by DCs and the cargo is released into the cytosol, we next analyzed the efficiency of cG^{S}A^{S}MP-loaded LNPs in activating STING signaling. Upon activation, STING becomes phosphorylated, enabling the initiation of inflammatory downstream signaling.[16−18] Western blot analysis revealed that p-STING is already detected after 4 h of incubation of DCs with cG^{S}A^{S}MP LNPs (Supplementary Figure 2B) and further accumulates up to 22 h. On the other hand, stimulation of DCs with free cG^{S}A^{S}MP results in very weak STING phosphorylation even after 22 h (Figure 2**D**), highlighting the effectiveness of the LNP formulation. Through immunofluorescence staining we confirmed that p-STING strongly accumulates in DCs exposed to cG^{S}A^{S}MP LNPs for 18 h (Figure 2**C**) but not in cG^{S}A^{S}MP-treated DCs. Consistent with these results, expression of the STING signaling-related target type I interferon IFNβ (IFNB) and the downstream target CXCL10, known to facilitate recruitment of CD8$^+$ T cells to tumor sites, was also significantly upregulated in cells treated with cG^{S}A^{S}MP LNPs for 22 h (Figure 2**E**) compared to free cG^{S}A^{S}MP.[54,55] Overall, these data indicate that cG^{S}A^{S}MP LNPs enable robust STING signaling in human DCs, whereas the same concentration of free cG^{S}A^{S}MP in solution fails to elicit any significant response.

3.3. cG^{S}A^{S}MP Loading Enhances STING-Mediated DC Activation. To assess whether loading of the STING agonist into LNPs enhances its capacity to activate DCs, surface marker expression of and cytokine secretion by cGAMP LNP treated DCs was analyzed. We first performed dose titration studies and found that incubating cells with cG^{S}A^{S}MP LNPs at a concentration corresponding to 15 μg/mL of lipids induced the highest secretion of the pro-inflammatory cytokines IL-6 and IL-12, while also increasing the expression of the costimulatory and maturation markers CD40, CD86 and HLA-DR (Supplementary Figure 3A and 3B). As a control, we assessed how free LNPs and free cG^{S}A^{S}MP (1.5 ± 0.3 μg/mL, calculated from a concentration of 15 μg/mL of lipids and the respective LNP loading efficiency) performed in activating DCs, at the highest tested dose of LNPs. Notably, the increased secretion of classical pro-inflammatory cytokines IL-6 and TNFα observed upon stimulation with cG^{S}A^{S}MP LNPs, was neither matched upon treatment with empty LNPs nor by cG^{S}A^{S}MP alone (Supplementary Figure 4A). A synergetic activating effect of cG^{S}A^{S}MP-loaded LNPs in DCs was further observed in the prominent increase of expression of CD86, HLA-DR and PD-L1 (Figure 2F). This effect was observed in an extended panel of markers to allow a thorough characterization of DCs incubated with cG^{S}A^{S}MP LNPs (Supplementary Figure 4C). Overall, both the free form of the STING

https://doi.org/10.1021/acsomega.5c06105
ACS Omega 2025, 10, 58465−58479

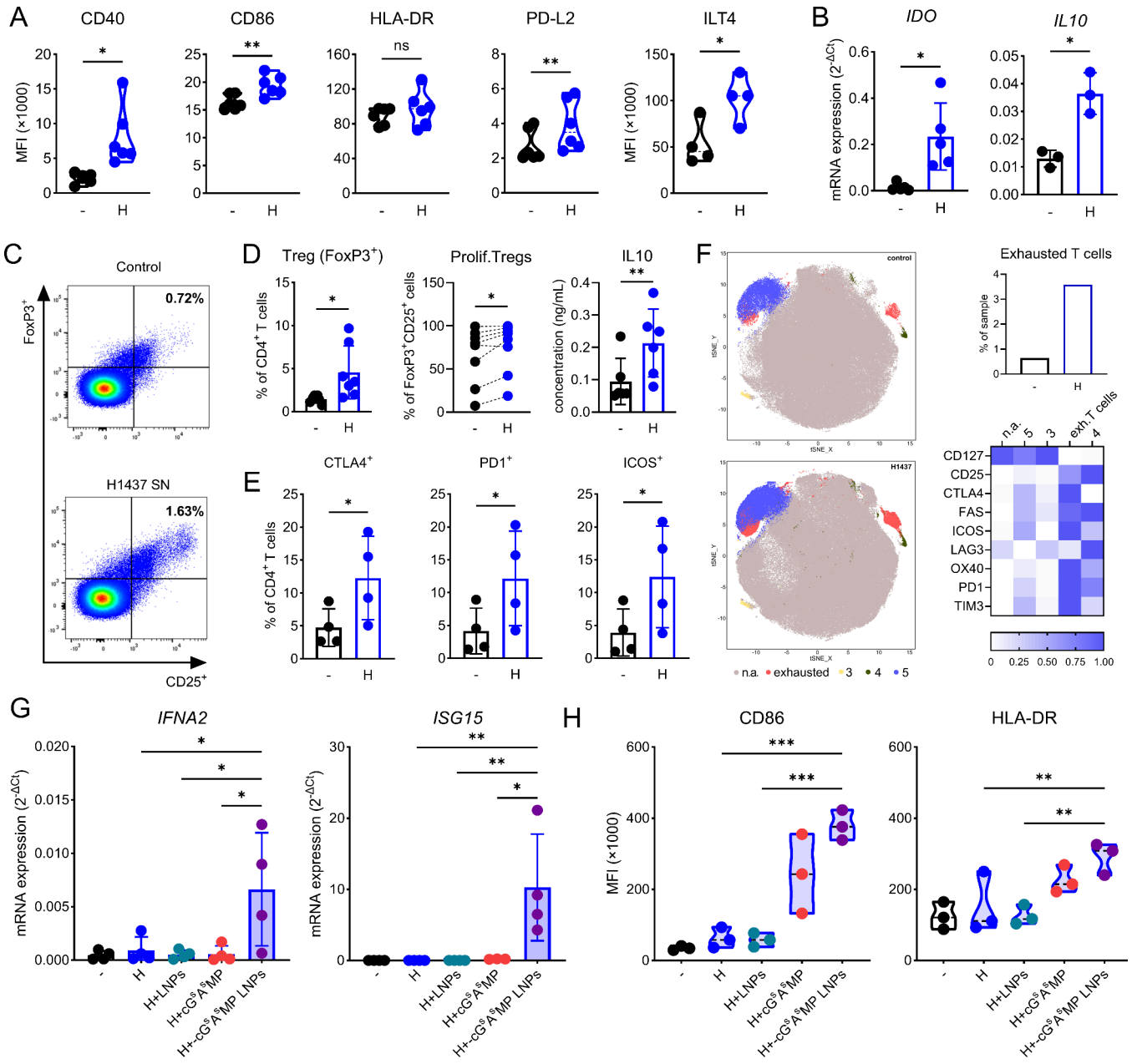

Figure 3. cG^{S}A^{S}MP LNPs trigger cellular responses in an *in vitro* model that mimics the phenotype of tumor-associated regulatory DCs (mregDC). Supernatants from human lung cancer cell lines modulate the DC phenotype and induce a clear regulatory T cell phenotype. (A) Differential surface marker expression and (B) IL10 and IDO gene expression of DCs after 24 h of treatment with cancer cell SNs (-: control, H: H1437 SN). (C) Representative gating strategy for identification of regulatory T cell (FoxP3$^+$CD25$^+$) population induced by six-day coculture of DCs treated with H1437 supernatant and with CD4$^+$ naïve T cells. (D) Percentages of Tregs, proliferating Tregs and IL-10 cytokine secretion of six-day cocultures. Additionally, (E) percentages of CTLA4$^+$, PD1$^+$ and ICOS$^+$ Tregs were analyzed in the pool of CD4$^+$ T-cells. (F) Multidimensional analysis of T cell subsets and respective cluster prevalence based on normalized expression of classical immuno-onco exhaustion T cell markers for three-day cocultures of DCs conditioned with H1437 supernatants and with CD4$^+$ naïve T cells. (G) Upregulation of STING activation target IFNA2 and downstream target ISG15. (H) Effects of free cG^{S}A^{S}MP and cG^{S}A^{S}MP LNPs in modulating expression of costimulatory and maturation markers of mregDCs. In panels (a), (b), (d), and (e), the values plotted represent the mean ± s.d. of individual donors. For statistical analysis, a two-tailed paired *t* test was performed. In g and h, values plotted of two independent experiments using two different LNP batches for a total of 3 individual donors. Statistical analysis was performed using RM-ANOVA with Tukey post hoc test. *$p \leq 0.05$, **$p \leq 0.01$, *** $p \leq 0.001$).

activator and the empty LNPs failed to induce significant effects on the modulation of cytokine secretion and surface marker expression in DCs, indicating that the potent effect of cG^{S}A^{S}MP LNPs is indeed due to efficient STING activation likely mediated by endosomal escape of cG^{S}A^{S}MP. Interestingly, whereas free cG^{S}A^{S}MP significantly lowered cell viability, encapsulation of the STING agonist in LNPs appears to mitigate the intrinsic toxicity of free cG^{S}A^{S}MP to DCs (Supplementary Figure 4B). The absence of a negative impact of these LNPs on cell viability is possibly related to the overall neutral charge of the nanoparticles, as the ionizable lipid does not impart a positive charge at physiological pH, which is often associated with cytotoxicity.[56]

https://doi.org/10.1021/acsomega.5c06105
ACS Omega 2025, 10, 58465−58479

3.4. cG^{S}A^{S}MP LNPs Trigger Cell Activation in an *In Vitro* Model of Cancer-Associated DCs. *3.4.1. In Vitro Model of Tumor-Associated Regulatory DCs (mregDCs).* To evaluate the potential of cG^{S}A^{S}MP LNPs in cancer immunotherapy, we developed an *in vitro* model that recapitulates an immunosuppressive DC phenotype observed in cancer patients. The immunosuppressive cues produced by the TME of solid tumors, such as in nonsmall cell lung cancer (NSCLC), have long been known to modulate immune cells and bring a halt to antitumor immune responses.[6] Accordingly, a subtype of mature but regulatory (mreg) DCs, which can differentiate from cDC1 as well as cDC2, have been described.[41] mreg DCs express both maturation and inhibitory molecules and have been identified in NSCLC patients, and later in patients afflicted with other cancers.[9,41] To mimic this mreg DC phenotype, we cultured DCs isolated from healthy donors with supernatants of the H1437 lung cancer cell line. DCs conditioned with cancer cell supernatants showed increased expression of costimulatory markers such as CD40 and CD86, with no change in HLA-DR (MHC II) (Figure 3**A**). Additionally, the coinhibitory markers PD-L2 and ILT4 were significantly elevated compared to untreated counterparts (Figure 3**A**).[57] At the gene-expression level, the supernatants induced upregulation of the anti-inflammatory cytokine IL-10 and indoleamine 2,3-dioxygenase (IDO), an enzyme that metabolizes tryptophan to kynurenine, and DCs expressing IDO are well-known to suppress potent T cell responses (Figure 3**B**).[58] Accordingly, mregDCs induced increased polarization and proliferation of CD4$^+$FoxP3$^+$CD25$^+$ regulatory T (Treg) cells (Figure 3**C and D**) and enhanced secretion of the immunosuppressive cytokine IL-10 in allogeneic DC/T cell cocultures (Figure 3**D**). Moreover, CD4$^+$ T cells displayed increased expression of the typical exhaustion T cell markers CTLA4, PD1 and ICOS, further confirming the increased presence of immunosuppressive Tregs in cultures with mregDCs (Figure 3**E**). These findings were corroborated by using cytometry by time-of-flight (CyTOF) analysis. Multidimensional clustering analysis revealed that T cells cocultured with mregDCs had a higher prevalence of CD4$^+$T cells with low expression of IL-7 receptor (CD127) and upregulated expression of the aforementioned traditional exhaustion markers, including CTLA-4, PD-1, ICOS and also OX40 (Figure 3**F**). Overall, these data suggest that DCs conditioned with supernatants from NSCLC cancer cells mimic the mregDC phenotype potentially driving Treg cell polarization analogously to that observed in cancer patients.[9,41,59−62]

3.4.2. cG^{s}A^{s}MP LNPs Activate mregDCs. The development of an *in vitro* model that recapitulates the phenotype of mregDCs in NSCLC provides a valuable platform to investigate the application of cG^{S}A^{S}MP LNPs as an adjuvant for future cancer immunotherapies. Notably, we found that cG^{S}A^{S}MP LNPs are highly efficient at activating STING-induced signaling in mregDCs, as evidenced by the significant increase of *ISG15* and *IFNA2* gene expression (Figure 3**G**).[63,64] The increase in STING-induced inflammatory responses occurs in concert with increased CD86 and HLA-DR levels on the DC surface after stimulation with cG^{S}A^{S}MP LNPs, suggesting that cG^{S}A^{S}MP LNPs can restore an active DC state (Figure 3**H**). Collectively, these data highlight the promising potential of cG^{S}A^{S}MP LNPs to activate DC-mediated inflammatory processes even in the face of an immunosuppressive TME.

4. DISCUSSION

In recent years, cGAS-STING signaling has emerged as a promising target for novel cancer immunotherapies, since STING activation is vital for potent antitumor immune responses.[65] Modulation of immune responses via activation of the STING pathway is carried out by different tissues and cell types.[66] In cancer cells, recent studies have reported that this pathway can directly trigger cell apoptosis and prompt the release of tumor antigens.[16] In addition to cancer cells, STING activation also induces type I IFN production by endothelial cells, facilitating the entrance of T cells into the bloodstream and their infiltration into the TME.[67] At the T-cell level, it has been reported that T-cell priming is severely impaired in STING-deficient mice compared to wild-type mice.[20,67] However, it is at the APC level that STING signaling appears to be critical in directing antitumor T-cell responses. Following uptake of tumor-derived DNA or native cGAMP by DCs, these cells express type I IFN and initiate adaptive antitumor immunity through DC-mediated T-cell cross-priming.[68,69] Consistent with this view, analysis of the transcriptional profile of intratumoral DCs in regressing tumors in mice revealed an activated state in conventional type 2 DCs that is marked by the expression of IFN-stimulated genes (ISG). These ISG$^+$DCs play a pivotal role in promoting antitumor immunity.[19] Nevertheless, despite the highly potent effect of CDNs as STING agonists in antitumor immunity, their efficacy and success strongly rely on a suitable drug delivery method. In fact, the administration of CDN-based STING agonist ADU-S100 in its free form resulted in low tumoricidal activity, thereby resulting in its exclusion from clinical trials (NCT03937141, NCT02675439, NCT03172936).[70] To tackle this setback, several nanocarriers have been tested for delivery of cGAMP or analogs to APCs in various *in vitro* or *in vivo* models, but to our knowledge, the potential of ionizable LNPs employed in COVID-19 vaccine as CDN carriers for STING agonism in human DCs has not yet been explored.[23,71] It is known that LNPs can complex with polyanionic cargos such as nucleic acids by electrostatic interactions with the positive charge provided by the ionizable lipid while achieving high yields in encapsulation.[36] Surprisingly, despite the small size and the only two negative charges of cG^{S}A^{S}MP, we obtained highly reproducible LNP batches with high encapsulation efficiency, which also outcompeted other nanobased CDN formulations in terms of shelf-stability (Figure 1.[33,72−75] Owing to the low-cost, well-documented safety profile across a large population, and easily accessible synthesis process, these LNPs have great potential for scalability through the use of commercially available microfluidic systems.[33,72,76] We show here that the STING agonist cG^{S}A^{S}MP has a potent effect in activating DCs and that LNPs act as an effective delivery vehicle and promote the release of the cargo into the cytoplasm, thereby potentiating the adjuvant effect of cG^{s}A^{s}MP (Figure 2. LNPs overcome the bottleneck of low endosomal release to some extent because of the ionizable nature of their constituent lipids, which can respond to the pH of the environment.[36,77] As a result of acidification during the endosomal maturation process, the ionizable lipid imparts a positive charge to the LNP which enables its binding to the negative lipids on the endosomal membrane, disrupting the membrane's structure.[78] Choice of helper lipids, ionizable lipids and sterol derivatives was further explored to enhance the performance of **cG^{s}A^{s}MP** showing that the LNPs

https://doi.org/10.1021/acsomega.5c06105
ACS Omega 2025, 10, 58465−58479

formulated as described in this work are possibly the most effective formulation (Supplementary Figure 6).

During the clinical development of LNPs for the COVID-19 vaccine, these nanoparticles were found to have adjuvant properties.[79,80] Yet, the mechanisms, or the exact cell type, that cause this effect are not known in detail. In this work, we observed that DCs treated with LNPs in the absence of any STING activator remained in a state comparable to that of control cells (Supplementary Figure 4), suggesting that other immune cells or specific interactions of certain immune cell types may be required to promote the adjuvant effect of LNPs. On the other hand, treatment of DCs with the free STING agonist led to moderate activation of these cells, while encapsulation of this CDN in LNPs strongly promoted an activated and mature phenotype, with high expression levels of CD40, CD80, CD86 and HLA-DR (Figure 2**F and**Supplementary Figure 4A and 4C)**.**[30,32,81] Although the human primary DCs herein used closely mimic physiological DCs and are thereby useful for high-throughput screening of novel molecules, single-culture *in vitro* systems are associated with limited biological relevance, particularly in the case of disease.[82−84] To address this obstacle, we established a novel system based on human primary DCs that can be tweaked to mimic the phenotype of TME-associated DCs, to test potential novel antitumor drug targets. Within the cancer context, the TME of solid tumors such as NSCLC modulates surrounding immune cells toward an unresponsive state and subdues the antitumor activity of DCs, further supporting tumor progression. Commonly, this TME-associated DC population is identified as being tolerogenic due to upregulation of coinhibitory molecules such as PD-L1, IDO, or ILT4 and IL10 and concomitant downregulation of classical pro-inflammatory and maturation markers such as TNFα and MHC II, respectively.[59,85,86] However, as identified by Maier et al. in single-cell RNA-sequenced samples of immune cells from tumors of NSCLC patients, tumor-associated DCs differ from traditional tolerogenic DCs in that they express both PD-L2 and CD40, conferring them a mature regulatory phenotype.[41] This is clearly in line with the phenotype we observed for mregDCs generated *in vitro*, where both traditional tolerogenic molecules and the maturation markers CD40 an CD86 are upregulated (Figure 3**.A).** mregDCs also showed upregulation of immunoregulatory molecules, including PD-L2, which binds to PD1 on T cell lymphocytes with a 3-fold stronger affinity than PD-L1, and ILT4, which is known to be upregulated in DCs exposed to immunosuppressive factors and to exert its inhibitory function upon binding MHC I molecules, competing with CD8 during $CD8^+$ T cell priming.[85,87] The altered phenotype of TME-associated mregDCs has been reported to impact functional outcomes of the T-cell response in antitumor immunity.[41,88,89] In fact, in 2001, Woo et al. reported for the first time that $CD4^+CD25^+$ Treg populations are highly represented in tumor-infiltrating lymphocytes of NSCLC patients and this was linked with antitumor immune anergy.[90] Consistent with clinical data, the findings we present here show increased polarization into Tregs in coculture with mregDCs, with increased expression of classical exhaustion markers such as ICOS, PD-1 and CTLA4, which are druggable targets in cancer immunotherapies and linked to poor prognosis in lung cancer patients (Figure 3**.C−F**).[91,92] As CTLA4 has a much higher affinity to CD80/86, the higher expression of CD86 observed in mregDCs may actually prompt an inhibitory pathway, since upregulation of CTLA4 in cocultures with $CD4^+$T cells was also observed.[93] Consistent with the immune-evasive phenotype, we observed higher secretion of IL-10 by T cells upon coculture with mregDCs, which is a mechanism used by Tregs to induce peripheral tolerance and actively suppress other lymphocyte populations as well as inhibit the function of DCs.[94,95] Since mregDCs present in the TME may contain tumor antigens, reprogramming these cells into a pro-inflammatory state emerges as a compelling strategy, particularly in poorly immunogenic tumors. One current strategy to engage DCs in antitumor responses is to induce immunogenic cancer cell death by chemotherapy and radiotherapy, with subsequent release of danger signals such as ATP or HMGB1.[96,97] Another approach is the use of adjuvants that trigger different PRRs in DCs (such as TLR3 and TLR5) or the use of CD40-activating antibodies that also facilitate maturation of mregDCs.[98,99] However, given its multifaceted role in antitumor immunity, STING is deemed a pivotal receptor to target for reprogramming of mregDCs.[32,100,101] Accordingly, our results show that stimulation of human mregDCs *in vitro* with cG^sA^sMP LNPs rescues an active and mature phenotype of DCs, giving encouraging results in engaging immune cells suppressed by the TME (Figure 3**.G-H**). By using primary human DCs and *in vitro*-conditioned DCs as a clinically relevant and translational model, this study presents an advanced test system that accurately reflects human biology and closely mimics the tumor microenvironment of lung cancer, providing complementary data to mouse systems that often fail to capture human-specific immune dynamics. Nevertheless, for additional *in vivo* studies or even clinical testing of novel carriers containing CDN-based STING agonists it is also essential to explore different routes of administration. Currently, most studies use intratumoral delivery, which limits the application to accessible solid tumors and thus does not unlock the full therapeutic potential of STING activation in immune cells.

5. CONCLUSIONS

This study highlights the potential of clinically approved LNPs as a promising nanocarriers for cytosolic delivery of CDN-based STING agonists into DCs. Compared to other types of nanoparticles, LNPs have the great advantage that they are highly reproducible and cost-effective, have already been tested across a large population, and are well suited for large-scale production. We showed that encapsulation of the STING agonist cG^sA^sMP in LNPs boosts its adjuvant effects in DCs and potentiates the activation of STING signaling, which is critical for potent antitumor responses. In addition, we presented a novel *in vitro* platform of human tumor-associated mregDCs that mirrors the phenotype of DCs isolated from tumors of cancer patients. The application of cG^sA^sMP LNPs to this model successfully reprograms mregDCs toward an active state, underscoring the potential of these nanocarriers for cancer immunotherapy. Collectively, these findings lay the groundwork for future research aimed at optimizing LNP-based approaches to enhance antitumor immune responses and to overcome hurdles associated with immune suppression.

■ ASSOCIATED CONTENT

Data Availability Statement

The data is available throughout the manuscript and supporting files. Raw data supporting the conclusions of this article will be made available by the authors upon reasonable request.

https://doi.org/10.1021/acsomega.5c06105
ACS Omega 2025, 10, 58465−58479

Supporting Information

The Supporting Information is available free of charge at https://pubs.acs.org/doi/10.1021/acsomega.5c06105.

Encapsulation efficiency and stability studies of cGsAsMP LNPs (Figure S1); endosomal escape of cGsAsMP LNPs and pSTING accumulation in DCs (Figure S2); dose titration of cGsAsMP LNPs in DCs (Figure S3); cGsAsMP LNPs induce activation of DCs in vitro (Figure S4); gating strategy for DC/CD4+ T cells cocultures (Figure S5); (Table S1) LNP formulations used in this study; LNP formulations encapsulation, uptake, release, and IFN production (Figure S6) (PDF)

AUTHOR INFORMATION

Corresponding Authors

Pascal Jonkheijm − *Department of Molecules and Materials, TechMed Centre and MESA+ Institute, University of Twente, Enschede 7500 AE, The Netherlands;* orcid.org/0000-0001-6271-0049; Email: p.jonkheijm@utwente.nl

Roberto Fiammengo − *Department of Biotechnology, University of Verona, Verona 37134, Italy;* orcid.org/0000-0002-6087-6851; Email: roberto.fiammengo@univr.it

Jutta Horejs-Hoeck − *Department of Biosciences and Medical Biology, Paris Lodron University of Salzburg, Salzburg 5020, Austria; Cancer Cluster Salzburg (CCS), Salzburg 5020, Austria;* orcid.org/0000-0002-0984-204X; Email: jutta.horejs-hoeck@plus.ac.at

Authors

Ana RS Ribeiro − *Department of Biosciences and Medical Biology, Paris Lodron University of Salzburg, Salzburg 5020, Austria; Cancer Cluster Salzburg (CCS), Salzburg 5020, Austria*

Ander Eguskiza − *Department of Biotechnology, University of Verona, Verona 37134, Italy; Department of Molecules and Materials, TechMed Centre and MESA+ Institute, University of Twente, Enschede 7500 AE, The Netherlands*

Hieu-Hoa Dang − *Department of Biosciences and Medical Biology, Paris Lodron University of Salzburg, Salzburg 5020, Austria; Cancer Cluster Salzburg (CCS), Salzburg 5020, Austria*

Theresa Neuper − *Department of Biosciences and Medical Biology, Paris Lodron University of Salzburg, Salzburg 5020, Austria; Cancer Cluster Salzburg (CCS), Salzburg 5020, Austria*

Michael Stefan Unger − *Department of Biosciences and Medical Biology, Paris Lodron University of Salzburg, Salzburg 5020, Austria; Cancer Cluster Salzburg (CCS), Salzburg 5020, Austria*

Laura Rodriguez Comas − *Department of Molecules and Materials, TechMed Centre and MESA+ Institute, University of Twente, Enschede 7500 AE, The Netherlands*

Markus Steiner − *Cancer Cluster Salzburg (CCS), Salzburg 5020, Austria; Department of Internal Medicine III with Haematology, Medical Oncology, Haemostaseology, Infectiology and Rheumatology, Oncologic Center, Salzburg Cancer Research Institute - Laboratory for Immunological and Molecular Cancer Research (SCRI-LIMCR), Paracelsus Medical University Salzburg, 5020 Salzburg, Austria;* orcid.org/0000-0003-4424-6347

Helene Sieberer − *Department of Biosciences and Medical Biology, Paris Lodron University of Salzburg, Salzburg 5020, Austria; Cancer Cluster Salzburg (CCS), Salzburg 5020, Austria*

Nadja Zaborsky − *Cancer Cluster Salzburg (CCS), Salzburg 5020, Austria; Department of Internal Medicine III with Haematology, Medical Oncology, Haemostaseology, Infectiology and Rheumatology, Oncologic Center, Salzburg Cancer Research Institute - Laboratory for Immunological and Molecular Cancer Research (SCRI-LIMCR), Paracelsus Medical University Salzburg, 5020 Salzburg, Austria*

Richard Greil − *Cancer Cluster Salzburg (CCS), Salzburg 5020, Austria; Department of Internal Medicine III with Haematology, Medical Oncology, Haemostaseology, Infectiology and Rheumatology, Oncologic Center, Salzburg Cancer Research Institute - Laboratory for Immunological and Molecular Cancer Research (SCRI-LIMCR), Paracelsus Medical University Salzburg, 5020 Salzburg, Austria*

Mireia Vilar I Hernandez − *Department of Molecules and Materials, TechMed Centre and MESA+ Institute, University of Twente, Enschede 7500 AE, The Netherlands;* orcid.org/0000-0002-8303-9060

Complete contact information is available at: https://pubs.acs.org/10.1021/acsomega.5c06105

Author Contributions

‡A.R.S.R. and A.E. shared first authorship.

Author Contributions

A.R.S.R. and A.E. contributed equally to the conceptualization and design of the work presented here, with A.E., L.R.C. and M.V.I.H. producing and characterizing LNPs and A.R.S.R. performing biological studies, with important support from H.H.D. M.S.U. conducted the uptake studies using confocal microscopy and H.S. performed the Western blot assays. M.S. performed the CyTOF data acquisition and analysis. T.N., P.J., R.F. and J.H.H. were key contributors to the concept and design of the project as well as data discussion with input from R.G. and N.Z. Finally, A.R.S.R. and A.E. wrote the manuscript and all coauthors have contributed to its revision and have approved the version to be published.

Notes

The authors declare no competing financial interest.

ACKNOWLEDGMENTS

We acknowledge our funding bodies; the European Union's Horizon 2020 research and innovation program under the Marie Skłodowska-Curie Action − Innovative Training Network DIRNANO (grant agreement no. 956544). Additional funding for this project was granted by the County of Salzburg, Cancer Cluster Salzburg [grant number 20102-P1601064-FPR01-2017], the Austrian Science Fund (FWF) [grant number P33969], the Biomed Center Salzburg (project 20102-F1901165-KZP), by the Priority program ACBN, University of Salzburg, and TKI ChemistryNL of the Dutch Ministry of Economic Affairs and Climate [grant number CHEMIE.PGT.2023.017].

REFERENCES

(1) June, C. H.; O'Connor, R. S.; Kawalekar, O. U.; Ghassemi, S.; Milone, M. C. CAR T cell immunotherapy for human cancer. *Science* **2018**, *359* (6382), 1361−1365.

(2) Arora, S.; Velichinskii, R.; Lesh, R. W.; Ali, U.; Kubiak, M.; Bansal, P.; Borghaei, H.; Edelman, M. J.; Boumber, Y. Existing and Emerging Biomarkers for Immune Checkpoint Immunotherapy in Solid Tumors. *Adv. Ther.* **2019**, *36*, 2638−2678.
(3) Wculek, S. K.; Cueto, F. J.; Mujal, A. M.; Melero, I.; Krummel, M. F.; Sancho, D. Dendritic cells in cancer immunology and immunotherapy. *Nat. Rev. Immunol.* **2020**, *20* (1), 7−24.
(4) Murphy, T. L.; Murphy, K. M. Dendritic cells in cancer immunology. *Cell. Mol. Immunol.* **2022**, *19* (1), 3−13.
(5) Paulis, L. E.; Mandal, S.; Kreutz, M.; Figdor, C. G. Dendritic cell-based nanovaccines for cancer immunotherapy. *Cur. Opin. Immunol.* **2013**, *25* (3), 389−395.
(6) Plesca, I.; Müller, L.; Böttcher, J. P.; Medyouf, H.; Wehner, R.; Schmitz, M. Tumor-associated human dendritic cell subsets: Phenotype, functional orientation, and clinical relevance. *Eur. J. Immunol.* **2022**, *52* (11), 1750−1758.
(7) Tay, R. E.; Richardson, E. K.; Toh, H. C. Revisiting the role of CD4+ T cells in cancer immunotherapy-new insights into old paradigms. *Cancer Gene Ther.* **2021**, *28* (1−2), 5−17.
(8) Janikashvili, N.; Bonnotte, B.; Katsanis, E.; Larmonier, N. The Dendritic Cell-Regulatory T Lymphocyte Crosstalk Contributes to Tumor-Induced Tolerance. *Clin. Dev. Immunol.* **2011**, *2011*, No. 430394.
(9) Li, J.; Zhou, J.; Huang, H.; Jiang, J.; Zhang, T.; Ni, C. Mature dendritic cells enriched in immunoregulatory molecules (mregDCs): A novel population in the tumour microenvironment and immunotherapy target. *Clin. Transl. Med.* **2023**, *13* (2), No. e1199.
(10) Gerhard, G. M.; Bill, R.; Messemaker, M.; Klein, A. M.; Pittet, M. J. Lipid metabolism and cancer. *J. Exp. Med.* **2021**, *218* (1), No. e20201606.
(11) Ziegler-Heitbrock, L.; Ancuta, P.; Crowe, S.; Dalod, M.; Grau, V.; Hart, D. N.; Leenen, P. J. M.; Liu, Y.-J.; MacPherson, G.; Randolph, G. J.; Scherberich, J.; Schmitz, J.; Shortman, K.; Sozzani, S.; Strobl, H.; Zembala, M.; Austyn, J. M.; Lutz, M. B. Nomenclature of monocytes and dendritic cells in blood. *Blood* **2010**, *116*, e74−e80.
(12) Böttcher, J. P.; Reis e Sousa, C. The Role of Type 1 Conventional dendritic cells in cancer immunity. *Trends Cancer* **2018**, *4*, 784−792.
(13) Nizzoli, G.; Krietsch, J.; Weick, A.; Steinfelder, S.; Facciotti, F.; Gruarin, P.; Bianco, A.; Steckel, B.; Moro, M.; Crosti, M.; Romagnani, C.; Stölzel, K.; Torretta, S.; Pignataro, L.; Scheibenbogen, C.; Neddermann, P.; De Francesco, R.; Abrignani, S.; Geginat, J. Human CD1c+ dendritic cells secrete high levels of IL-12 and potently prime cytotoxic T-cell responses. *Blood* **2013**, *122* (6), 932−942.
(14) Ruhland, M. K.; Roberts, E. W.; Cai, E.; Mujal, A. M.; Marchuk, K.; Beppler, C.; Nam, D.; Serwas, N. K.; Binnewies, M.; Krummel, M. F. Visualizing synaptic transfer of tumor antigens among dendritic cells. *Cancer Cell* **2020**, *37* (6), 786−799.
(15) Cai, X.; Chiu, Y.-H.; Chen, Z. J. The cGAS-cGAMP-STING pathway of cytosolic DNA sensing and signaling. *Mol. Cell* **2014**, *54* (2), 289−296.
(16) Zhu, Y.; An, X.; Zhang, X.; Qiao, Y.; Zheng, T.; Li, X. STING: a master regulator in the cancer-immunity cycle. *Mol. Cancer* **2019**, *18* (1), 1−15.
(17) Marcus, A.; Mao, A. J.; Lensink-Vasan, M.; Wang, L.; Vance, R. E.; Raulet, D. H. Tumor-Derived cGAMP Triggers a STING-Mediated Interferon Response in Non-tumor Cells to Activate the NK Cell Response. *Immunity* **2018**, *49* (4), 754−763.
(18) Luteijn, R. D.; Zaver, S. A.; Gowen, B. G.; Wyman, S. K.; Garelis, N. E.; Onia, L.; McWhirter, S. M.; Katibah, G. E.; Corn, J. E.; Woodward, J. J.; Raulet, D. H. SLC19A1 transports immunoreactive cyclic dinucleotides. *Nature* **2019**, *573* (7774), 434−438.
(19) Duong, E.; Fessenden, T. B.; Lutz, E.; Dinter, T.; Yim, L.; Blatt, S.; Bhutkar, A.; Wittrup, K. D.; Spranger, S. Type I interferon activates MHC class I-dressed CD11b+ conventional dendritic cells to promote protective anti-tumor CD8+ T cell immunity. *Immunity* **2022**, *55* (2), 308−323. e9.
(20) Woo, S. R.; Fuertes, M. B.; Corrales, L.; Spranger, S.; Furdyna, M. J.; Leung, M. Y. K.; Duggan, R.; Wang, Y.; Barber, G. N.; Fitzgerald, K. A.; Alegre, M. L.; Gajewski, T. F. STING-dependent cytosolic DNA sensing mediates innate immune recognition of immunogenic tumors. *Immunity* **2014**, *41* (5), 830−842.
(21) Wang-Bishop, L.; Kimmel, B. R.; Ngwa, V. M.; Madden, M. Z.; Baljon, J. J.; Florian, D. C.; Hanna, A.; Pastora, L. E.; Sheehy, T. L.; Kwiatkowski, A. J.; Wehbe, M.; Wen, X.; Becker, K. W.; Garland, K. M.; Schulman, J. A.; Shae, D.; Edwards, D.; Wolf, M. M.; Delapp, R.; Christov, P. P.; Beckermann, K. E.; Balko, J. M.; Rathmell, W. K.; Rathmell, J. C.; Chen, J.; Wilson, J. T. STING-activating nanoparticles normalize the vascular-immune interface to potentiate cancer immunotherapy. *Sci. Immunol.* **2023**, *8* (83), No. eadd1153.
(22) Zhang, H.; You, Q.-D.; Xu, X.-L. Targeting Stimulator of Interferon Genes (STING): A Medicinal Chemistry Perspective. *J. Med. Chem.* **2020**, *63* (8), 3785−3816.
(23) Garland, K. M.; Sheehy, T. L.; Wilson, J. T. Chemical and Biomolecular Strategies for STING Pathway Activation in Cancer Immunotherapy. *Chem. Rev.* **2022**, *122* (6), 5977−6039.
(24) Carozza, J. A.; Cordova, A. F.; Brown, J. A.; AlSaif, Y.; Böhnert, V.; Cao, X.; Mardjuki, R. E.; Skariah, G.; Fernandez, D.; Li, L. ENPP1's regulation of extracellular cGAMP is a ubiquitous mechanism of attenuating STING signaling. *Proc. Natl. Acad. Sci. U.S.A.* **2022**, *119* (21), No. e2119189119.
(25) Motedayen Aval, L.; Pease, J. E.; Sharma, R.; Pinato, D. J. Challenges and Opportunities in the Clinical Development of STING Agonists for Cancer Immunotherapy. *J. Clin. Med.* **2020**, *9* (10), 3323.
(26) Riley, R. S.; June, C. H.; Langer, R.; Mitchell, M. J. Delivery technologies for cancer immunotherapy. *Nat. Rev. Drug Discovery* **2019**, *18* (3), 175−196.
(27) Yang, M.; Li, J.; Gu, P.; Fan, X. The application of nanoparticles in cancer immunotherapy: Targeting tumor microenvironment. *Bioact. Mater.* **2021**, *6* (7), 1973−1987.
(28) Ou, B. S.; Saouaf, O. M.; Yan, J.; Bruun, T. U. J.; Baillet, J.; Zhou, X.; King, N. P.; Appel, E. A. Broad and Durable Humoral Responses Following Single Hydrogel Immunization of SARS-CoV-2 Subunit Vaccine. *Adv. Healthc. Mater.* **2023**, *12* (28), No. 2301495.
(29) Wang, J.; Li, P.; Yu, Y.; Fu, Y.; Jiang, H.; Lu, M.; Sun, Z.; Jiang, S.; Lu, L.; Wu, M. X. Pulmonary surfactant-biomimetic nanoparticles potentiate heterosubtypic influenza immunity. *Science* **2020**, *367* (6480), No. eaau0810.
(30) Park, K. S.; Xu, C.; Sun, X.; Louttit, C.; Moon, J. J. Improving STING Agonist Delivery for Cancer Immunotherapy Using Biodegradable Mesoporous Silica Nanoparticles. *Adv. Therap.* **2020**, *3* (10), No. 2000130.
(31) Janjua, T. I.; Cao, Y.; Yu, C.; Popat, A. Clinical translation of silica nanoparticles. *Nat. Rev. Mater.* **2021**, *6* (12), 1072−1074.
(32) Shae, D.; Becker, K. W.; Christov, P.; Yun, D. S.; Lytton-Jean, A. K. R.; Sevimli, S.; Ascano, M.; Kelley, M.; Johnson, D. B.; Balko, J. M.; Wilson, J. T. Endosomolytic polymersomes increase the activity of cyclic dinucleotide STING agonists to enhance cancer immunotherapy. *Nat. Nanotechnol.* **2019**, *14* (3), 269−278.
(33) Koshy, S. T.; Cheung, A. S.; Gu, L.; Graveline, A. R.; Mooney, D. J. Liposomal Delivery Enhances Immune Activation by STING Agonists for Cancer Immunotherapy. *Adv. Biosyst.* **2017**, *1* (1−2), No. 1600013.
(34) Dane, E. L.; Belessiotis-Richards, A.; Backlund, C.; Wang, J.; Hidaka, K.; Milling, L. E.; Bhagchandani, S.; Melo, M. B.; Wu, S.; Li, N.; Donahue, N.; Ni, K.; Ma, L.; Okaniwa, M.; Stevens, M. M.; Alexander-Katz, A.; Irvine, D. J. STING agonist delivery by tumour-penetrating PEG-lipid nanodiscs primes robust anticancer immunity. *Nat. Mater.* **2022**, *21* (6), 710−720.
(35) Nakamura, T.; Sato, T.; Endo, R.; Sasaki, S.; Takahashi, N.; Sato, Y.; Hyodo, M.; Hayakawa, Y.; Harashima, H. STING agonist loaded lipid nanoparticles overcome anti-PD-1 resistance in melanoma lung metastasis via NK cell activation. *J. Immunother. Cancer* **2021**, *9* (7), No. e002852.
(36) Hou, X.; Zaks, T.; Langer, R.; Dong, Y. Lipid nanoparticles for mRNA delivery. *Nat. Rev. Mater.* **2021**, *6* (12), 1078−1094.
(37) Tenchov, R.; Bird, R.; Curtze, A. E.; Zhou, Q. Lipid Nanoparticles—From Liposomes to mRNA Vaccine Delivery, a

https://doi.org/10.1021/acsomega.5c06105
ACS Omega 2025, 10, 58465−58479

Landscape of Research Diversity and Advancement. *ACS Nano* **2021**, *15* (11), 16982−17015.
(38) Agency, E. M. *Spikevax Asessment Report EMA/896245/2022*; https://www.ema.europa.eu/en/documents/variation-report/spikevax-previously-covid-19-vaccine-moderna-h-c-005791-ii-0075-g-epar-assessment-report-variation_en.pdf, **2022**; p 191.
(39) Hejdankova, Z.; Vanek, V.; Sedlak, F.; Prochazka, J.; Diederichs, A.; Kereïche, S.; Novotna, B.; Budesinsky, M.; Birkus, G.; Grantz Saskova, K.; Cigler, P. Lipid Nanoparticles for Broad-Spectrum Nucleic Acid Delivery. *Adv. Funct. Mater.* **2021**, *31* (47), No. 2101391.
(40) Shaji, S. G.; Patel, P.; Mamani, U.-F.; Guo, Y.; Koirala, S.; Lin, C.-Y.; Alahmari, M.; Omoscharka, E.; Cheng, K. Delivery of a STING agonist using lipid nanoparticles inhibits pancreatic cancer growth. *Int. J. Nanomedicine* **2024**, *19*, 8769−8778.
(41) Maier, B.; Leader, A. M.; Chen, S. T.; Tung, N.; Chang, C.; LeBerichel, J.; Chudnovskiy, A.; Maskey, S.; Walker, L.; Finnigan, J. P.; Kirkling, M. E.; Reizis, B.; Ghosh, S.; D'Amore, N. R.; Bhardwaj, N.; Rothlin, C. V.; Wolf, A.; Flores, R.; Marron, T.; Rahman, A. H.; Kenigsberg, E.; Brown, B. D.; Merad, M. A conserved dendritic-cell regulatory program limits antitumour immunity. *Nature* **2020**, *580* (7802), 257−262.
(42) Wang, X.; Liu, S.; Sun, Y.; Yu, X.; Lee, S. M.; Cheng, Q.; Wei, T.; Gong, J.; Robinson, J.; Zhang, D.; Lian, X.; Basak, P.; Siegwart, D. J. Preparation of selective organ-targeting (SORT) lipid nanoparticles (LNPs) using multiple technical methods for tissue-specific mRNA delivery. *Nat. Protoc.* **2023**, *18* (1), 265−291.
(43) Schwarz, H.; Gornicec, J.; Neuper, T.; Parigiani, M. A.; Wallner, M.; Duschl, A.; Horejs-Hoeck, J. Biological Activity of Masked Endotoxin. *Sci. Rep.* **2017**, *7* (1), 44750.
(44) Neuper, T.; Frauenlob, T.; Sarajlic, M.; Posselt, G.; Wessler, S.; Horejs-Hoeck, J. TLR2, TLR4 and TLR10 Shape the Cytokine and Chemokine Release of H. pylori-Infected Human DCs. *Int. J. Mol. Sci.* **2020**, *21* (11), 3897.
(45) Connors, J.; Joyner, D.; Mege, N. J.; Cusimano, G. M.; Bell, M. R.; Marcy, J.; Taramangalam, B.; Kim, K. M.; Lin, P. J. C.; Tam, Y. K.; Weissman, D.; Kutzler, M. A.; Alameh, M. G.; Haddad, E. K. Lipid nanoparticles (LNP) induce activation and maturation of antigen presenting cells in young and aged individuals. *Commun. Biol.* **2023**, *6* (1), 188.
(46) Hammill, D. CytoExploreR: Interactive analysis of cytometry data *R package version 2020* 2021, *1* (8).
(47) Ashhurst, T. M.; Marsh-Wakefield, F.; Putri, G. H.; Spiteri, A. G.; Shinko, D.; Read, M. N.; Smith, A. L.; King, N. J. C. Integration, exploration, and analysis of high-dimensional single-cell cytometry data using Spectre. *Cytometry A* **2022**, *101* (3), 237−253.
(48) Li, L.; Yin, Q.; Kuss, P.; Maliga, Z.; Millán, J. L.; Wu, H.; Mitchison, T. J. Hydrolysis of 2'3'-cGAMP by ENPP1 and design of nonhydrolyzable analogs. *Nat. Chem. Biol.* **2014**, *10* (12), 1043−1048.
(49) Schwarz, H.; Schmittner, M.; Duschl, A.; Horejs-Hoeck, J. Residual endotoxin contaminations in recombinant proteins are sufficient to activate human CD1c+ dendritic cells. *PloS One* **2014**, *9* (12), No. e113840.
(50) Akinc, A.; Querbes, W.; De, S.; Qin, J.; Frank-Kamenetsky, M.; Jayaprakash, K. N.; Jayaraman, M.; Rajeev, K. G.; Cantley, W. L.; Dorkin, J. R.; Butler, J. S.; Qin, L.; Racie, T.; Sprague, A.; Fava, E.; Zeigerer, A.; Hope, M. J.; Zerial, M.; Sah, D. W.; Fitzgerald, K.; Tracy, M. A.; Manoharan, M.; Koteliansky, V.; Fougerolles, A. d.; Maier, M. A. Targeted delivery of RNAi therapeutics with endogenous and exogenous ligand-based mechanisms. *Mol. Ther.* **2010**, *18* (7), 1357−1364.
(51) Mellman, I. Endocytosis and molecular sorting. *Annu. Rev. Cell Dev. Biol.* **1996**, *12* (1), 575−625.
(52) Schlich, M.; Palomba, R.; Costabile, G.; Mizrahy, S.; Pannuzzo, M.; Peer, D.; Decuzzi, P. Cytosolic delivery of nucleic acids: The case of ionizable lipid nanoparticles. *Bioeng. Transl. Med.* **2021**, *6* (2), No. e10213.
(53) Stirpe, F.; Olsnes, S.; Pihl, A. Gelonin, a new inhibitor of protein synthesis, nontoxic to intact cells. Isolation, characterization, and preparation of cytotoxic complexes with concanavalin A. *J. Biol. Chem.* **1980**, *255*, 6947−6953.
(54) Kabelitz, D.; Zarobkiewicz, M.; Heib, M.; Serrano, R.; Kunz, M.; Chitadze, G.; Adam, D.; Peters, C. Signal strength of STING activation determines cytokine plasticity and cell death in human monocytes. *Sci. Rep.* **2022**, *12* (1), 17827.
(55) Spranger, S.; Dai, D.; Horton, B.; Gajewski, T. F. Tumor-Residing Batf3 Dendritic Cells Are Required for Effector T Cell Trafficking and Adoptive T Cell Therapy. *Cancer Cell* **2017**, *31* (5), 711−723. e4.
(56) Jörgensen, A. M.; Wibel, R.; Bernkop-Schnürch, A. Biodegradable Cationic and Ionizable Cationic Lipids: A Roadmap for Safer Pharmaceutical Excipients. *Small* **2023**, *19* (17), No. 2206968.
(57) Gao, A.; Sun, Y.; Peng, G. ILT4 functions as a potential checkpoint molecule for tumor immunotherapy. *BBA Reviews on Cancer* **2018**, *1869* (2), 278−285.
(58) Mellor, A. L.; Munn, D. H. IDO expression by dendritic cells: tolerance and tryptophan catabolism. *Nat. Rev. Immunol.* **2004**, *4* (10), 762−774.
(59) Domogalla, M. P.; Rostan, P. V.; Raker, V. K.; Steinbrink, K. Tolerance through Education: How Tolerogenic Dendritic Cells Shape Immunity. *Front. Immunol.* **2017**, *8*, 1764.
(60) Manni, G.; Mondanelli, G.; Scalisi, G.; Pallotta, M. T.; Nardi, D.; Padiglioni, E.; Romani, R.; Talesa, V. N.; Puccetti, P.; Fallarino, F.; Gargaro, M. Pharmacologic Induction of Endotoxin Tolerance in Dendritic Cells by L-Kynurenine. *Front. Immunol.* **2020**, *11*, 292.
(61) Cella, M.; Döhring, C.; Samaridis, J.; Dessing, M.; Brockhaus, M.; Lanzavecchia, A.; Colonna, M. A novel inhibitory receptor (ILT3) expressed on monocytes, macrophages, and dendritic cells involved in antigen processing. *J. Exp. Med.* **1997**, *185* (10), 1743−1751.
(62) Lavin, Y.; Kobayashi, S.; Leader, A.; Amir, E. a. D.; Elefant, N.; Bigenwald, C.; Remark, R.; Sweeney, R.; Becker, C. D.; Levine, J. H.; Meinhof, K.; Chow, A.; Kim-Shulze, S.; Wolf, A.; Medaglia, C.; Li, H.; Rytlewski, J. A.; Emerson, R. O.; Solovyov, A.; Greenbaum, B. D.; Sanders, C.; Vignali, M.; Beasley, M. B.; Flores, R.; Gnjatic, S.; Pe'er, D.; Rahman, A.; Amit, I.; Merad, M. Innate Immune Landscape in Early Lung Adenocarcinoma by Paired Single-Cell Analyses. *Cell* **2017**, *169* (4), 750−765. e17.
(63) Sun, L.; Wu, J.; Du, F.; Chen, X.; Chen, Z. J. Cyclic GMP-AMP synthase is a cytosolic DNA sensor that activates the type I interferon pathway. *Science* **2013**, *339* (6121), 786−791.
(64) Li, X.-D.; Wu, J.; Gao, D.; Wang, H.; Sun, L.; Chen, Z. J. Pivotal roles of cGAS-cGAMP signaling in antiviral defense and immune adjuvant effects. *Science* **2013**, *341* (6152), 1390−1394.
(65) Kwon, J.; Bakhoum, S. F. The Cytosolic DNA-Sensing cGAS-STING Pathway in Cancer. *Cancer Discovery* **2020**, *10* (1), 26−39.
(66) Sundararaman, S. K.; Barbie, D. A. Tumor cGAMP Awakens the Natural Killers. *Immunity* **2018**, *49* (4), 585−587.
(67) Demaria, O.; De Gassart, A.; Coso, S.; Gestermann, N.; Di Domizio, J.; Flatz, L.; Gaide, O.; Michielin, O.; Hwu, P.; Petrova, T. V.; Martinon, F.; Modlin, R. L.; Speiser, D. E.; Gilliet, M. STING activation of tumor endothelial cells initiates spontaneous and therapeutic antitumor immunity. *Proc. Natl. Acad. Sci. U.S.A.* **2015**, *112* (50), 15408−15413.
(68) Diamond, M. S.; Kinder, M.; Matsushita, H.; Mashayekhi, M.; Dunn, G. P.; Archambault, J. M.; Lee, H.; Arthur, C. D.; White, J. M.; Kalinke, U.; Murphy, K. M.; Schreiber, R. D. Type I interferon is selectively required by dendritic cells for immune rejection of tumors. *J. Exp. Med.* **2011**, *208* (10), 1989−2003.
(69) Deng, L.; Liang, H.; Xu, M.; Yang, X.; Burnette, B.; Arina, A.; Li, X. D.; Mauceri, H.; Beckett, M.; Darga, T.; Huang, X.; Gajewski, T. F.; Chen, Z. J.; Fu, Y. X.; Weichselbaum, R. R. STING-Dependent Cytosolic DNA Sensing Promotes Radiation-Induced Type I Interferon-Dependent Antitumor Immunity in Immunogenic Tumors. *Immunity* **2014**, *41* (5), 843−852.
(70) Meric-Bernstam, F.; Sweis, R. F.; Kasper, S.; Hamid, O.; Bhatia, S.; Dummer, R.; Stradella, A.; Long, G. V.; Spreafico, A.; Shimizu, T.; Steeghs, N.; Luke, J. J.; McWhirter, S. M.; Müller, T.; Nair, N.; Lewis,

https://doi.org/10.1021/acsomega.5c06105
ACS Omega 2025, 10, 58465−58479

N.; Chen, X.; Bean, A.; Kattenhorn, L.; Pelletier, M.; Sandhu, S. Combination of the STING Agonist MIW815 (ADU-S100) and PD-1 Inhibitor Spartalizumab in Advanced/Metastatic Solid Tumors or Lymphomas: An Open-Label, Multicenter. *Phase Ib Study. Clin. Cancer Res.* **2023**, *29* (1), 110−121.
(71) Zhao, K.; Huang, J.; Zhao, Y.; Wang, S.; Xu, J.; Yin, K. Targeting STING in cancer: Challenges and emerging opportunities. *Biochim. Biophys. Acta Rev. on Cancer* **2023**, *1878*, No. 188983.
(72) Hanson, M. C.; Crespo, M. P.; Abraham, W.; Moynihan, K. D.; Szeto, G. L.; Chen, S. H.; Melo, M. B.; Mueller, S.; Irvine, D. J. Nanoparticulate STING agonists are potent lymph node-targeted vaccine adjuvants. *J. Clin. Invest.* **2015**, *125* (6), 2532−2546.
(73) Doshi, A. S.; Cantin, S.; Prickett, L. B.; Mele, D. A.; Amiji, M. Systemic nano-delivery of low-dose STING agonist targeted to CD103+ dendritic cells for cancer immunotherapy. *J. Controlled Release* **2022**, *345*, 721−733.
(74) Atukorale, P. U.; Raghunathan, S. P.; Raguveer, V.; Moon, T. J.; Zheng, C.; Bielecki, P. A.; Wiese, M. L.; Goldberg, A. L.; Covarrubias, G.; Hoimes, C. J.; Karathanasis, E. Nanoparticle Encapsulation of Synergistic Immune Agonists Enables Systemic Codelivery to Tumor Sites and IFNβ-Driven Antitumor Immunity. *Cancer Res.* **2019**, *79* (20), 5394−5406.
(75) Meng, C.; Chen, Z.; Li, G.; Welte, T.; Shen, H. Nanoplatforms for mRNA Therapeutics. *Adv. Therap.* **2021**, *4* (1), No. 2000099.
(76) Nakamura, T.; Miyabe, H.; Hyodo, M.; Sato, Y.; Hayakawa, Y.; Harashima, H. Liposomes loaded with a STING pathway ligand, cyclic di-GMP, enhance cancer immunotherapy against metastatic melanoma. *J. Controlled Release* **2015**, *216*, 149−157.
(77) Zheng, L.; Bandara, S. R.; Tan, Z.; Leal, C. Lipid nanoparticle topology regulates endosomal escape and delivery of RNA to the cytoplasm. *Proc. Natl. Acad. Sci. U.S.A.* **2023**, *120* (27), No. e2301067120.
(78) Cullis, P. R.; Hope, M. J. Lipid Nanoparticle Systems for Enabling Gene Therapies. *Mol. Ther.* **2017**, *25* (7), 1467−1475.
(79) Walsh, E. E.; Frenck, R. W.; Falsey, A. R.; Kitchin, N.; Absalon, J.; Gurtman, A.; Lockhart, S.; Neuzil, K.; Mulligan, M. J.; Bailey, R.; Swanson, K. A.; Li, P.; Koury, K.; Kalina, W.; Cooper, D.; Fontes-Garfias, C.; Shi, P. Y.; Türeci, Ö.; Tompkins, K. R.; Lyke, K. E.; Raabe, V.; Dormitzer, P. R.; Jansen, K. U.; Şahin, U.; Gruber, W. C. Safety and Immunogenicity of Two RNA-Based Covid-19 Vaccine Candidates. *N. Engl. J. Med.* **2020**, *383* (25), 2439−2450.
(80) Baden, L. R.; El Sahly, H. M.; Essink, B.; Kotloff, K.; Frey, S.; Novak, R.; Diemert, D.; Spector, S. A.; Rouphael, N.; Creech, C. B.; McGettigan, J.; Khetan, S.; Segall, N.; Solis, J.; Brosz, A.; Fierro, C.; Schwartz, H.; Neuzil, K.; Corey, L.; Gilbert, P.; Janes, H.; Follmann, D.; Marovich, M.; Mascola, J.; Polakowski, L.; Ledgerwood, J.; Graham, B. S.; Bennett, H.; Pajon, R.; Knightly, C.; Leav, B.; Deng, W.; Zhou, H.; Han, S.; Ivarsson, M.; Miller, J.; Zaks, T. Efficacy and Safety of the mRNA-1273 SARS-CoV-2 Vaccine. *N. Engl. J. Med.* **2021**, *384* (5), 403−416.
(81) Li, K.; Ye, Y.; Liu, L.; Sha, Q.; Wang, X.; Jiao, T.; Zhang, L.; Wang, J. The lipid platform increases the activity of STING agonists to synergize checkpoint blockade therapy against melanoma. *Biomater. Sci.* **2021**, *9* (3), 765−773.
(82) Boraschi, D.; Li, D.; Li, Y.; Italiani, P. In Vitro and In Vivo Models to Assess the Immune-Related Effects of Nanomaterials. *Int. J. Environ. Res. Public Health* **2021**, *18* (22), 11769.
(83) Santegoets, S. J.; van den Eertwegh, A. J.; van de Loosdrecht, A. A.; Scheper, R. J.; de Gruijl, T. D. Human dendritic cell line models for DC differentiation and clinical DC vaccination studies. *J. Leukoc. Biol.* **2008**, *84* (6), 1364−1373.
(84) Robbins, S. H.; Walzer, T.; Dembélé, D.; Thibault, C.; Defays, A.; Bessou, G.; Xu, H.; Vivier, E.; Sellars, M.; Pierre, P.; Sharp, F. R.; Chan, S.; Kastner, P.; Dalod, M. Novel insights into the relationships between dendritic cell subsets in human and mouse revealed by genome-wide expression profiling. *Genome Biol.* **2008**, *9*, 1−27.
(85) Ju, X.-S.; Hacker, C.; Scherer, B.; Redecke, V.; Berger, T.; Schuler, G.; Wagner, H.; Lipford, G. B.; Zenke, M. Immunoglobulin-like transcripts ILT2, ILT3 and ILT7 are expressed by human dendritic cells and down-regulated following activation. *Gene* **2004**, *331*, 159−164.
(86) Terness, P.; Bauer, T. M.; Röse, L.; Dufter, C.; Watzlik, A.; Simon, H.; Opelz, G. The Inhibition of allogeneic T cell proliferation by indoleamine 2,3-dioxygenase-expressing dendritic cells: mediation of suppression by tryptophan metabolites. *J. Exp. Med.* **2002**, *196* (4), 447−457.
(87) Shiroishi, M.; Tsumoto, K.; Amano, K.; Shirakihara, Y.; Colonna, M.; Braud, V. M.; Allan, D. S. J.; Makadzange, A.; Rowland-Jones, S.; Willcox, B.; Jones, E. Y.; van der Merwe, P. A.; Kumagai, I.; Maenaka, K. Human inhibitory receptors Ig-like transcript 2 (ILT2) and ILT4 compete with CD8 for MHC class I binding and bind preferentially to HLA-G. *Proc. Natl. Acad. Sci. U.S.A.* **2003**, *100* (15), 8856−8861.
(88) Minohara, K.; Imai, M.; Matoba, T.; Wing, J. B.; Shime, H.; Odanaka, M.; Uraki, R.; Kawakita, D.; Toyama, T.; Takahashi, S.; Morita, A.; Murakami, S.; Ohkura, N.; Sakaguchi, S.; Iwasaki, S.; Yamazaki, S. Mature dendritic cells enriched in regulatory molecules may control regulatory T cells and the prognosis of head and neck cancer. *Cancer Sci.* **2023**, *114* (4), 1256.
(89) Jonuleit, H.; Schmitt, E.; Steinbrink, K.; Enk, A. H. Dendritic cells as a tool to induce anergic and regulatory T cells. *Trends Immunol.* **2001**, *22* (7), 394−400.
(90) Woo, E. Y.; Chu, C. S.; Goletz, T. J.; Schlienger, K.; Yeh, H.; Coukos, G.; Rubin, S. C.; Kaiser, L. R.; June, C. H. Regulatory CD4(+)CD25(+) T cells in tumors from patients with early-stage non-small cell lung cancer and late-stage ovarian cancer. *Cancer Res.* **2001**, *61* (12), 4766−4772.
(91) Wu, Y.; Du, B.; Lin, M.; Ji, X.; Lv, C.; Lai, J. The identification of genes associated T-cell exhaustion and construction of prognostic signature to predict immunotherapy response in lung adenocarcinoma. *Sci. Rep.* **2023**, *13* (1), 13415.
(92) Beyer, M.; Schultze, J. L. Regulatory T cells in cancer. *Blood* **2006**, *108* (3), 804−811.
(93) Takahashi, T.; Tagami, T.; Yamazaki, S.; Uede, T.; Shimizu, J.; Sakaguchi, N.; Mak, T. W.; Sakaguchi, S. Immunologic self-tolerance maintained by CD25(+)CD4(+) regulatory T cells constitutively expressing cytotoxic T lymphocyte-associated antigen 4. *J. Exp. Med.* **2000**, *192* (2), 303−310.
(94) Mittal, S. K.; Roche, P. A. Suppression of antigen presentation by IL-10. *Curr. Opin. Immunol.* **2015**, *34*, 22−27.
(95) Sadeghzadeh, M.; Bornehdeli, S.; Mohahammadrezakhani, H.; Abolghasemi, M.; Poursaei, E.; Asadi, M.; Zafari, V.; Aghebati-Maleki, L.; Shanehbandi, D. Dendritic cell therapy in cancer treatment; the state-of-the-art. *Life Sci.* **2020**, *254*, No. 117580.
(96) Fucikova, J.; Kepp, O.; Kasikova, L.; Petroni, G.; Yamazaki, T.; Liu, P.; Zhao, L.; Spisek, R.; Kroemer, G.; Galluzzi, L. Detection of immunogenic cell death and its relevance for cancer therapy. *Cell Death Dis.* **2020**, *11* (11), 1013.
(97) Ashrafizadeh, M.; Farhood, B.; Eleojo Musa, A.; Taeb, S.; Najafi, M. Damage-associated molecular patterns in tumor radiotherapy. *Int. Immunopharmacol.* **2020**, *86*, No. 106761.
(98) Scarlett, U. K.; Cubillos-Ruiz, J. R.; Nesbeth, Y. C.; Martinez, D. G.; Engle, X.; Gewirtz, A. T.; Ahonen, C. L.; Conejo-Garcia, J. R. In situ stimulation of CD40 and Toll-like receptor 3 transforms ovarian cancer-infiltrating dendritic cells from immunosuppressive to immunostimulatory cells. *Cancer Res.* **2009**, *69* (18), 7329−7337.
(99) Cubillos-Ruiz, J. R.; Engle, X.; Scarlett, U. K.; Martinez, D.; Barber, A.; Elgueta, R.; Wang, L.; Nesbeth, Y.; Durant, Y.; Gewirtz, A. T.; Sentman, C. L.; Kedl, R.; Conejo-Garcia, J. R. Polyethylenimine-based siRNA nanocomplexes reprogram tumor-associated dendritic cells via TLR5 to elicit therapeutic antitumor immunity. *J. Clin. Invest.* **2009**, *119* (8), 2231−2244.
(100) Cheng, N.; Watkins-Schulz, R.; Junkins, R. D.; David, C. N.; Johnson, B. M.; Montgomery, S. A.; Peine, K. J.; Darr, D. B.; Yuan, H.; McKinnon, K. P.; Liu, Q.; Miao, L.; Huang, L.; Bachelder, E. M.; Ainslie, K. M.; Ting, J. P. Y. A nanoparticle-incorporated STING activator enhances antitumor immunity in PD-L1−insensitive models

https://doi.org/10.1021/acsomega.5c06105
ACS Omega 2025, 10, 58465−58479

of triple-negative breast cancer. *JCI Insight* **2018**, *3* (22), No. e120638.
(101) Longhi, M. P.; Trumpfheller, C.; Idoyaga, J.; Caskey, M.; Matos, I.; Kluger, C.; Salazar, A. M.; Colonna, M.; Steinman, R. M. Dendritic cells require a systemic type I interferon response to mature and induce CD4+ Th1 immunity with poly IC as adjuvant. *J. Exp. Med.* **2009**, *206* (7), 1589−1602.

https://doi.org/10.1021/acsomega.5c06105
ACS Omega 2025, 10, 58465−58479